Free-Energy Dependence of Electron-Transfer Rate Constants at Si/Liquid Interfaces

Arnel M. Fajardo and Nathan S. Lewis*

Division of Chemistry and Chemical Engineering, California Institute of Technology, Pasadena, California 91125

Received: June 26, 1997; In Final Form: September 25, 1997[⊗]

Differential capacitance vs potential and current density vs potential measurements have been used to characterize the interfacial energetics and kinetics, respectively, of n-type Si electrodes in contact with a series of one-electron, outer-sphere redox couples. The differential capacitance data yielded values for the electron concentration at the surface of the semiconductor as well as values for the driving force of the interfacial electron-transfer event at Si/CH_3OH−viologen$^{2+/+}$ junctions. The differential capacitance vs potential measurements were essentially independent of the ac frequency imposed on the interface, with linear Bode plots (log|impedance| vs log frequency, at a fixed potential) between ≈10^3 and ≈10^5 Hz, with slopes typically between −0.99 and −1.00. The slopes of C^{-2}−E (Mott−Schottky) plots were in excellent agreement with theory, and little frequency dispersion was observed in the *x*-intercepts of such plots. The conduction band edge of the n-type Si anodes was invariant to within ±40 mV in response to a variation in the redox potential of the solution of greater than 400 mV, indicating "ideal" interfacial energetic behavior of this system with no evidence for Fermi level pinning. From these measurements, the surface-state density of the Si/CH_3OH contact can be estimated as $<10^{11}$ cm^2, i.e., less than 1 defect for 10^4 surface atoms. The current density vs potential plots exhibited a first-order kinetic dependence on the concentration of electrons at the semiconductor surface and a first-order kinetic dependence on the concentration of acceptors in the solution. Rate constants for transfer of charge from the semiconductor to the acceptor were determined as a function of the driving force for the interfacial charge-transfer event. The rate constants varied from 4×10^{-18} cm^4 s^{-1} to 6×10^{-17} cm^4 s^{-1} and were well fit to Marcus-type behavior, with a reorganization energy of 0.7 eV and a maximum rate constant at optimal exoergicity of 6×10^{-17} cm^4 s^{-1}. This maximum rate constant value is in excellent agreement with theoretical expectations for transfer of charge from a delocalized carrier in a semiconductor to a one-electron, outer-sphere redox acceptor dissolved in the electrolyte solution.

I. Background and Theory

Although Gerischer pointed out over 30 years ago that semiconductor electrodes possess significant advantages over metal electrodes in addressing many of the basic predictions of interfacial electron-transfer theories,[1] relatively few robust kinetic measurements have been reported for charge transfer from semiconductor electrodes to one-electron, outer-sphere redox species.[2−7] Such measurements have been thwarted by the poorly understood, nonideal behavior of most semiconductor/liquid contacts,[4,8] by the instability of semiconductor electrodes in aqueous electrolytes,[9,10] and by the inability to perform a systematic study of the interfacial kinetic processes for a homologous series of one-electron, outer-sphere redox systems having similar reorganization energies.

Recent work from our laboratory has shown that these drawbacks can be largely overcome through use of n-type Si electrodes in CH_3OH with a series of viologens as the soluble one-electron acceptors.[11] Si electrodes are stable toward passivation or corrosion reactions in dry methanol,[12,13] and the driving force for interfacial charge transfer can be varied in this solvent system through the use of a homologous series of viologen$^{2+/+}$ redox species.[14] Furthermore, such interfaces appear to exhibit simple and nearly ideal energetic and kinetic behavior.[11] The ability to vary the energetics for the interfacial charge-transfer event makes it possible to investigate the predictions of Marcus theory with regard to the variation in rate constant as a function of driving force at the semiconductor/liquid contact.[7,15,16] In addition, such measurements allow experimental determination of the maximum charge-transfer rate constant at optimal exoergicity for such contacts, thereby allowing an estimate of the electronic coupling between the delocalized charge carriers in the semiconductor electrode and the localized electron acceptors in the solution phase. In the present work, we provide full details of these kinetic measurements and report new results on the kinetic and energetic behavior of this set of semiconductor/liquid junctions.

A. Comparison between the Kinetic Behavior of Metallic and Semiconducting Electrodes. Because kinetic measurements at semiconductor electrodes have not been emphasized in the literature relative to measurements at metallic electrodes, it is useful to compare the behavior expected for the two different types of electrodes. We first summarize the expectations for a metal electrode and then discuss the kinetic situation for a semiconductor/liquid contact.

1. Metal Electrodes. For reduction of an acceptor at a metal electrode, the rate law for current flow is[17,18]

$$J(E) = -qk_m(E)[\mathrm{A}] \tag{1}$$

where J is the interfacial current density at an electrode potential E, q is the charge on the electron, [A] is the concentration (in units of molecules cm^{-3}) of redox acceptors at the interface, and $k_m(E)$ is the charge-transfer rate constant at the potential E. The rate constant $k_m(E)$ has units of cm s^{-1}. In this well-known rate law, the electron concentration at the surface of the metal, $n_{s,m}$, is not directly determined experimentally and is instead implicitly contained in the value of $k_m(E)$.

* To whom correspondence should be addressed.
[⊗] Abstract published in *Advance ACS Abstracts,* November 15, 1997.

S1089-5647(97)02087-7 CCC: $14.00

SCHEME 1: Thermodynamic and Kinetic Parameters of a Metal/Liquid Interface[a]

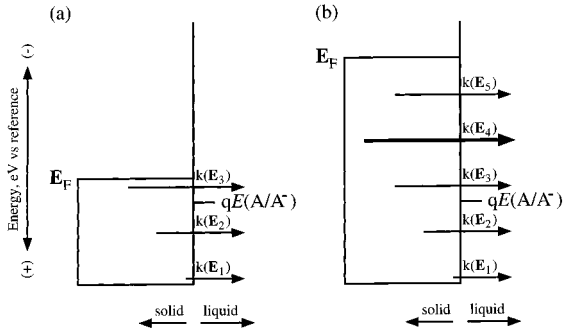

[a] $\mathbf{E}_F$ is the Fermi level of the metal, q is the electronic charge, and $qE(A/A^-)$ is the electrochemical potential of the solution. $k(\mathbf{E})$ is the electron-transfer rate constant at an energy $\mathbf{E}$, and the length of each associated arrow denotes the relative magnitude of the rate constant. The shaded area indicates occupied electronic states in the metal electrode. (a) In the normal Marcus regime, an increase in potential effects a larger observed rate, since larger rate constants are continually accessed. (b) In the inverted Marcus regime, an increase in potential does not result in a smaller observed rate, since the rate constant at optimal exoergicity (here represented by $k(\mathbf{E}_4)$) dominates the electron-transfer process.

SCHEME 2: Thermodynamic and Kinetic Parameters of a Semiconductor/Liquid Interface[a]

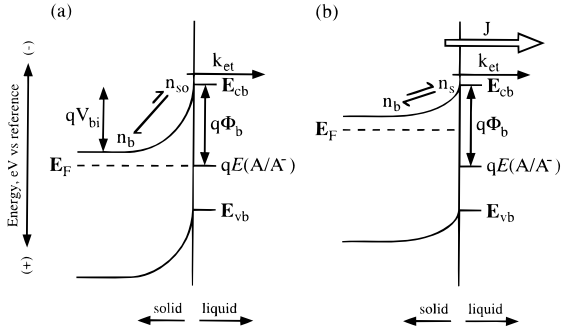

[a] $\mathbf{E}_{cb}$ and $\mathbf{E}_{vb}$ are, respectively, the conduction and valence band edge energies at the surface of the semiconductor, V_{bi} is the built-in voltage of the semiconductor/liquid contact, ϕ_b is the barrier height, and k_{et} is the electron-transfer rate constant. (a) At equilibrium, a Boltzmann distribution relates the electron concentration in the bulk of the semiconductor (n_b) to the equilibrium electron concentration at the surface (n_{so}). (b) As the junction is biased away from equilibrium, a current density (J) is observed because the electron concentration at the surface of the semiconductor (n_s) is larger than n_{so}. Unlike electron transfer across a metal/liquid interface, the experimental rate constant is invariant with potential.

The measured rate constant $k_m(E)$ is actually a summation of the energy-dependent rate constants that describe interfacial charge transfer from every occupied electronic state in the metal to the acceptor species in the solution phase. Every energy-dependent rate constant has its own activation energy and implicitly includes the electron concentration at the surface of the metal at that specific energy (Scheme 1a). Although neither the individual energy-dependent rate constants nor the electron concentrations included in these $k_m(E)$ values have been measured to date, the Marcus theory nevertheless does predict a functional form for the dependence of $k_m(E)$ on E, if the density of states in the metal is assumed to be independent of energy and if the electronic coupling between the charge carrier in the solid and the acceptor in the solution is also independent of energy.[19,20] Recent kinetic studies for redox species immobilized at a fixed distance in a self-assembled monolayer on a gold surface[19−22] and for freely diffusing species through insulating barrier layers on electrode surfaces[23] have verified this prediction, subject to these assumptions, in satisfying detail.

Another consequence of the kinetic behavior of a metal/electrolyte interface is that, at optimal exoergicity for a freely diffusing redox species at such a contact, the interfacial flux is always controlled by mass transport, not by kinetics. Because the electrode surface has such a large concentration of electrons that can participate in the interfacial charge-transfer process, the current density expected theoretically at optimal exoergicity far exceeds the mass-transport-limited flux of redox species to the electrode surface. This precludes direct measurement of $k_m(E)$ for such systems and requires either surface immobilization of the redox reagent[19] or the formation of insulating, nearly pinhole-free overlayers on the metal[23] in order to access the required rate constant regime. Also, Marcus inverted behavior for the individual energy-dependent values of $k_m(E)$ cannot be directly observed at a metal/electrolyte interface because there are always occupied electronic states at optimal exoergicity that dominate the interfacial current flow and maintain the optimal rate of charge transfer to the acceptor in the solution (Scheme 1b).

2. Semiconducting Electrodes. For a semiconductor electrode, the situation is quite different. For an n-type semiconductor in contact with a redox system A/A^- of formal reduction potential $E^{\circ\prime}(A/A^-)$, it is generally possible to identify systems in which the energies of the conduction and valence band edges at the surface of the semiconductor, $\mathbf{E}_{cb}$ and $\mathbf{E}_{vb}$ respectively, are very different from the value of $qE^{\circ\prime}(A/A^-)$. Since no electronic states are available in the forbidden energy gap of the semiconductor, only electrons that are thermally excited into the conduction band of the solid need to be considered in the kinetic rate expression for electron flow from the semiconductor into the solution (Scheme 2a). For electron transfer from the conduction band of the solid to the acceptor species in the solution, the charge-transfer rate law is therefore[7,15]

$$J(E) = -qk_{et}n_s[A] \tag{2}$$

where k_{et} is the second-order rate constant and n_s is the electron concentration at the surface of the semiconductor.

This kinetic behavior differs in several important aspects from that of a metal electrode. First, n_s is explicitly contained in the rate law and thus is not included in the value of k_{et}. The value of n_s can be determined experimentally and is related to the electron concentration in the bulk, n_b, through a Boltzmann relation:[24]

$$n_s = n_b \exp\{q(E_{fb} - E)/(kT)\} \tag{3}$$

where q is the electronic charge, k is Boltzmann's constant, T is temperature, and E_{fb} is the flat-band potential of the semiconductor. The value of the potential drop in the semiconductor electrode can be determined through a variety of methods,[24−27] and n_b can be measured from knowledge of the sample resistivity and the mobility of carriers in the solid.[24,28,29] Therefore, n_s is known in principle for any specific semiconductor/liquid interface. Since the diffusion coefficient of electrons in the semiconductor is much larger than the diffusion coefficient of ions in the solution phase,[18] exchange of electrons between the bulk and surface regions of the solid occurs very rapidly relative to interfacial charge transfer.[26,30] In fact, a limiting current density of 10^7 A cm^{-2} could, in principle, be supported at $E = E_{fb}$ before transport of charge carriers in the solid becomes rate-limiting.[24] Since this is much larger than any experimentally accessible current density in an electrochemical

experiment, the charge carrier transport process can be viewed chemically as a rapid preequilibrium followed by a rate-determining charge-transfer step. In this framework, the potential dropped in the semiconductor determines the electron concentration involved in the rate-determining process, n_s, in terms of its value in the bulk, n_b, through eq 3.

Second, the electrons available for charge transfer at a semiconductor/liquid contact are contained in a narrow region of defined, experimentally determinable energies. Because the valence electrons of dopant atoms must undergo thermal excitation to produce free carriers in the solid, to an excellent approximation, only electronic states with energies of ($\mathbf{E}_{cb} - 3kT$) < $\mathbf{E}$ < $\mathbf{E}_{cb}$ are occupied by free carriers.[31] Only these carriers can therefore contribute to the interfacial current flow that determines the value of k_{et}. The measured k_{et} for a semiconductor electrode thus corresponds more closely to a microscopic, individual-energy, interfacial charge-transfer rate constant than does $k_m(E)$ for a metal electrode, since the latter is integrated over a much wider energy range of occupied electronic states.

Third, changing the electrode potential does not affect the driving force for charge transfer at a semiconductor/liquid contact, and thus, k_{et} is essentially independent of E. Because the differential capacitance of a nondegenerately doped semiconductor electrode is much smaller than that of the Helmholtz layer in the electrolyte, an applied potential drops almost exclusively across the semiconductor electrode instead of across the double layer of such solid/liquid contacts.[1,15,18,24,32,33] Changing the electrode potential of a semiconductor/liquid contact therefore primarily affects the value of n_s and does not perturb k_{et} (Scheme 2b). In this fashion, the potential dependence of the current density at a semiconductor electrode allows direct evaluation of the first-order dependence of J on n_s (eq 2) and allows explicit removal of n_s from the observed kinetic rate to obtain a value for k_{et}. However, it is not possible to investigate the driving-force dependence of k_{et} through manipulation of the electrode potential; instead, the value of $\mathbf{E}_{cb}$ or of the formal reduction potential of the redox couple, $E^{\circ\prime}(A/A^-)$, must be manipulated at the semiconductor/liquid contact.

Fourth, because the electron concentration at the surface of the semiconductor electrode can be very small, typically 6−8 orders of magnitude less than the atomic density of the solid, even charge-transfer events that proceed at optimal exoergicity produce very small absolute interfacial charge carrier fluxes. For example, at an n-Si/liquid contact with $\mathbf{E}_{cb} - qE^{\circ\prime}(A/A^-) = -0.5$ eV, charge transfer at an optimally exoergic rate constant of 1×10^{-16} cm^4 s^{-1} would produce an exchange current density of only 10 μA cm^{-2} at [A] = 10 mM. This is far smaller than the mass-transport-limited value of 1900 μA cm^{-2} that would be obtained for this redox system at a rotating disk electrode of rotation velocity 100 rev min^{-1}.[18,34] Rate constants at optimal exoergicity therefore can be determined at semiconductor electrodes without interference from mass-transport limitations, which prevent measurement of the analogous kinetic processes at metal/liquid interfaces.

Finally, because of the limited energetic range of the occupied electronic states in the solid, it should be possible to observe directly the Marcus inverted region for interfacial charge transfer at a semiconductor/liquid interface. In fact, Fujishima et al. have interpreted the current−potential behavior at deuterated vs nondeuterated thianthrene cation radicals at ZnO electrodes within this type of inverted-region framework.[35] Transient absorbance data at the $TiO_2-Fe^{III}(CN)_5(ligand)^{x+}$ interface have also been cited as evidence for the Marcus inverted region.[36]

In this work, we have determined n_s, [A], and J experimentally for a series of Si/methanol contacts using redox species that have a relatively constant reorganization energy but that produce varying values of $\mathbf{E}_{cb} - qE^{\circ\prime}(A/A^-)$. In each system, the rate law of eq 2 was obeyed experimentally so that k_{et} could be computed. The data thus yielded values of k_{et} for transfer of delocalized electrons from a narrowly defined region of energy in the semiconductor to the redox acceptors in the solution. The observed dependence of k_{et} on $\mathbf{E}_{cb} - qE^{\circ\prime}(A/A^-)$ permits evaluation of the predicted dependence of the rate constant on the driving force for the interfacial charge-transfer event. Since the measurements have been performed for a redox species that is dissolved in homogeneous solution, these data necessarily involve an integration over distance between the acceptor and the interface, in contrast to the fixed-distance rate constant data that have been obtained recently by Chidsey and collaborators for charge transfer at metal/liquid interfaces.[19,20] The maximum value of k_{et} determined experimentally for the n-Si/CH_3OH contact also allows estimation of the electronic coupling between the delocalized electron in the solid and the electron acceptor in the solution phase and provides a basis for comparison of the experimental data to the predictions of theoretical models[7,16] for this charge-transfer process.

II. Experimental Section

A. Electrodes and Solutions. The n-type Si wafers (phosphorus-doped, (100)-orientation) were purchased from Silicon Sense, Inc. (Nashua, NH) and had resistivities of either 0.74 or 5.9 Ω cm. Resistivities were measured with a four-point probe and were converted into dopant densities via empirical relationships that have been published previously.[29] A Ga:In eutectic provided an ohmic contact to the n-Si, which was then attached to a Sn:Cu wire using conductive Ag print (GC Electronics). The n-Si wafer and Sn:Cu wire were sealed in a glass tube through use of white epoxy (Dexter Corp.). Photographs of the exposed Si areas alongside a microruler were digitized to determine the electrode areas, which were typically 0.75−0.85 cm^2.[37]

Before each electrochemical measurement, n-Si electrodes were etched in 48% HF(aq) (Mallinckrodt, Inc.), rinsed with 18 MΩ cm resistivity H_2O (from a Barnstead NANOPure filter), and dried with N_2(g). In addition, the Pt wire reference electrode and the Pt gauze counter electrode (Aldrich; 52 mesh, 5 cm^2) were cleaned in a 3:1 (v/v) solution of HCl(aq) (37% w/w, EM Science) and HNO_3(aq) (70% w/w, EM Science). The electrodes were then rinsed with 18 MΩ cm resistivity H_2O and dried under flowing N_2(g). All electrical measurements were conducted in a N_2(g)-purged Plexiglas box, which had less than 10 ppm of O_2 as monitored by the lack of fuming of $(CH_3CH_2)_2Zn$.

Methanol was obtained from EM Science and was distilled over Mg prior to use. Lithium chloride (EM Science) was dried under active vacuum for at least 6 h at 240 °C and was stored under N_2(g) until use. The electrolyte and redox compounds were maintained under N_2(g) while they were loaded into the cell vessel and dissolved into the solvent. All electrochemical cell solutions contained 1.0 M LiCl. The cation radicals of the bipyridinium compounds were created in situ via bulk electrolysis with a Pt gauze counter electrode separated from the main cell solution by a Vycor frit. Formal reduction potentials were taken to be the mean of the cyclic voltammetric peak potentials that were measured at a Pt wire in a CH_3OH−1.0 M LiCl solution containing 20 mM of the bipyridinium dication of interest. Nernstian solution potentials were monitored before and after each set of electrical measurements through use of a

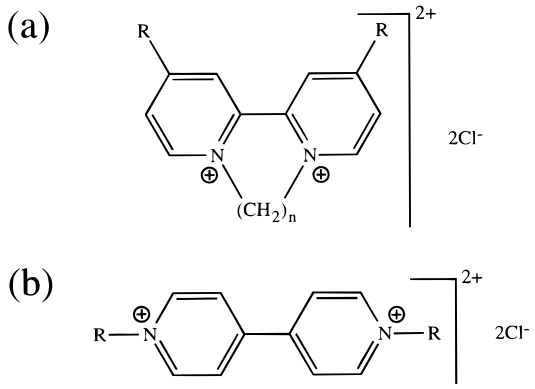

Figure 1. Structures of the seven bipyridinium compounds used in this work. Compounds **I**−**III** have the structure illustrated in (a), whereas compounds **IV**−**VII** have the structure shown in (b). Values of R and *n* for each reagent are given in Table 1, and specific preparative procedures are described in the text.

TABLE 1: Formal Reduction Potentials of Bipyridinium$^{2+/+}$ Cations[a]

redox compound	*n*	*R*	$E°'$(A/A$^-$), V vs SCE
I	3	H	−0.572
II	2	CH_3	−0.518
III	2	H	−0.399
IV		CH_3	−0.453
V		$CH_2C_6H_5$	−0.382
VI		$CH_2COOC_2H_5$	−0.296
VII		$CH(COOC_2H_5)_2$	−0.195

[a] The standard reduction potentials were obtained from cyclic voltammetric measurements at a Pt wire. Each solution for cyclic voltammetry consisted of 20 mM bipyridinium dication and 1.0 M LiCl in CH_3OH.

CH_3OH−LiCl saturated calomel reference electrode (SCE). The potential of this electrode was −0.050 V vs a standard aqueous SCE.

B. Redox Compounds. The structures of the seven redox compounds used in this work are given in Figure 1. For brevity, these compounds have been assigned numeric symbols that generally increase with more positive formal reduction potentials (Table 1). Methyl viologen dichloride (**IV**) hydrate and benzyl viologen dichloride (**V**) were purchased from Aldrich, Inc. and were dried under active vacuum for 6 h at 60 °C before use. The other bipyridinium compounds were synthesized according to the general Menschutkin reaction in which an amine is quaternized with an alkyl halide.[38] In this procedure, the dibromide salts were formed initially and (except for compound **VII**) were converted to the dichloride products by anion-exchange with a Sephadex DEAE A-50 resin. The preparative routes were obtained from the literature.[39,40] Acetone, diethyl ether, and Na_2CO_3 were obtained from EM Science, and all other reagents were purchased from Aldrich, Inc. All materials were used as received. Proton NMR spectra were obtained using a General Electric QE300 300 MHz spectrometer, and the chemical shifts are referenced to the residual proton peak of HOD.

*7,8-Dihydro-6H-dipyrido[1,2-a:2′,1′-c]-[1,4]-diazepinium Dichloride (**I**).* 2,2′-Dipyridyl (2 g) was dissolved in 1,3-dibromopropane (10 mL). The solution was stirred under reflux at 165 °C for 20 h. The resultant pale yellow dibromide precipitate was washed with acetone and converted to the dichloride salt in a CH_3OH solution. This solution was concentrated to 20 mL via rotary evaporation, and the product was recrystallized by addition of acetone. The crystals were rinsed with acetone and diethyl ether and were then dried under active vacuum for 2 h. ^{1}H NMR (D_2O) δ: CH_2, 3.4 (quintet); CH_2N^+, 5.1 (triplet); aromatic, 8.5 (multiplet), 8.6, 9.4 (doublet), 9.6 (doublet).

*6,7-Dihydro-2,11-dimethyldipyrido[1,2-a:2′,1′-c]pyrazinium Dichloride (**II**).* 1,2-Dibromoethane (3 mL) was added to a solution of 4,4′-dimethyl-2,2′-dipyridyl (3 g) in nitrobenzene (19 mL). The mixture was stirred at 170 °C for 10 h. The dull purple solid was collected and rinsed with acetone and diethyl ether. The dichloride salt was obtained as a CH_3OH solution, and the final product was recrystallized by addition of acetone. The crystals were washed with acetone and diethyl ether and were dried at 70 °C under active vacuum for 6 h. ^{1}H NMR (D_2O) δ: CH_3, 2.8; CH_2N^+, 5.2; aromatic, 8.2 (doublet), 8.8, 9.0 (doublet).

*6,7-Dihydrodipyrido[1,2-a:2′,1′-c]pyrazinium Dichloride (**III**).* 2,2′-Dipyridyl (2.83 g) was dissolved in 1,2-dibromoethane (14.2 mL). The solution was stirred under reflux at 130 °C for 17 h. The green-yellow precipitate was collected and rinsed with acetone and diethyl ether. The CH_3OH solution of the dichloride salt was reduced in volume via rotary evaporation, and addition of acetone induced recrystallization. The crystals were rinsed with acetone and were dried at 60 °C under active vacuum for 6 h. ^{1}H NMR (D_2O) δ: CH_2N^+, 5.4; aromatic, 8.4−9.0 (multiplet), 9.2 (doublet).

*1,1′-Bis(ethoxycarbonylmethyl)-4,4′-bipyridinium Dichloride (**VI**).* Ethyl bromoacetate (5 g) was added to a solution of 4,4′-dipyridyl (2 g) in acetonitrile (50 mL). The mixture was stirred under reflux at 90 °C for 48 h, and the resulting yellow dibromide salt was collected and rinsed with acetonitrile and diethyl ether. After the conversion to the dichloride compound, the final product was recrystallized from CH_3OH by addition of diethyl ether. After several rinses with diethyl ether, the collected crystals were dried for 3 h under active vacuum. ^{1}H NMR (D_2O) δ: CH_3, 1.3 (triplet); CH_2O, 4.3 (quartet); CH_2N^+, 5.7; aromatic, 8.6, 9.1 (both doublets).

*1,1′-Bis(diethoxycarbonylmethyl)-4,4′-bipyridinium Dichloride (**VII**).* Diethyl bromomalonate (5 mL) was added to a solution of 4,4′-dipyridyl (2 g) in absolute ethanol (10 mL). The reaction mixture was stirred at room temperature for 48 h, stirred under reflux for 4 h, and then allowed to return to room temperature. A saturated aqueous solution of Na_2CO_3 (10 mL) was added to the deep-red solution. The red precipitate was collected and rinsed with H_2O. This solid was dissolved in boiling *N*,*N*′-dimethylformamide, and insoluble material was removed by hot gravity filtration. Once the mixture had cooled to room temperature, the recrystallized solid was collected (2.0 g) and rinsed with diethyl ether. This intermediate product was suspended in CH_3OH and made soluble by addition of concentrated HCl(aq) (0.5 mL). Recrystallization of the final dichloride compound was induced by diethyl ether. The brown crystals were washed with diethyl ether and dried under active vacuum for 3 h. ^{1}H NMR (D_2O) δ: CH_3, 1.3 (triplet); CH_2, 4.4 (quartet); aromatic, 8.7, 9.3 (both doublets).

C. Electrical Measurements. After an HF-etched n-Si electrode was transferred into the N_2 atmosphere, the electrode was immersed for 2 min in a 0.2 M solution of ferrocenium tetrafluoroborate (available from previous work in this laboratory[41]) in CH_3OH, rinsed with CH_3OH, and dried in flowing N_2(g). This chemical treatment induced a reproducible flat-band shift, as reported in prior work,[14] and was found to result in stable and reproducible current density−potential (J−E) behavior at the n-Si/CH_3OH−bipyridinium$^{2+/+}$ interface. To ensure electrode stability, the semiconductor working electrode was cycled between +0.500 and −0.100 V vs the Nernstian solution potential E(A/A$^-$) for 30 min under ambient room illumination before use. Any unstable electrodes were then discarded. J−E properties were recorded before and

after the differential capacitance measurements. Both the steady-state $J-E$ behavior and the differential capacitance vs potential ($C^{-2}-E$) behavior were performed in the dark. $E(A/A^-)$ was measured before and after collection of the $J-E$ and $C^{-2}-E$ data.

$J-E$ data were obtained with an EG&G Princeton Applied Research Model 273 potentiostat and a Houston Instruments Omnigraphic 2000 $X-Y$ recorder. The scan rate was 50 mV s^{-1} in all experiments. The dark $J-E$ curves were digitized and were corrected for concentration overpotential and cell resistance losses by measuring the mass-transport-limited currents at a one-sided Pt foil electrode. For a given redox solution, the limiting anodic current density, $J_{l,a}$, and the limiting cathodic current density, $J_{l,c}$, at this Pt foil electrode were used with the current density J at an n-Si electrode to correct the Si $J-E$ data for any concentration overpotential η_{conc}:[18]

$$\eta_{conc} = \left(\frac{RT}{nF}\right)\left\{\ln\left(\frac{J_{1,a}}{-J_{1,c}}\right) - \ln\left(\frac{J_{1,a} - J}{J - J_{1,c}}\right)\right\} \quad (4)$$

where R is the gas constant, n is the number of electrons transferrred (one in this case), and F is the Faraday constant. The cell resistance R_{cell} was extracted from the high-frequency limits of the Bode plots of the n-Si/$CH_3OH-viologen^{2+/+}$ junctions. The final corrected potential, E_{corr}, was calculated from E, η_{conc}, R_{cell}, and the current i using the equation

$$E_{corr} = E - \eta_{conc} - iR_{cell} \quad (5)$$

The reference point of the potentials was then changed to SCE by accounting for the difference between $E(A/A^-)$ and SCE.

As observed previously, n-Si electrodes in contact with these viologen solutions exhibited stable $J-E$ characteristics within the typical measurement time scale of several hours.[11,14] For an individual cell, the cathodic currents at a given forward bias changed by less than 10% over the course of the differential capacitance experiments. For an entire series of Si/liquid contacts with each individual redox couple, the current density at a given potential was likewise constant to within ±10%. Cell stability was further verified by monitoring $E(A/A^-)$, which changed by no more than 3 mV from the beginning to the end of the $J-E$ and $C^{-2}-E$ measurements performed using a given electrode.

The differential capacitance experiments were performed on a Schlumberger Instruments Model 1260 impedance/gain-phase analyzer that was linked to a Model 1286 electrochemical interface. Both instruments were driven by computer control. A 10 mV ac signal was superimposed on the dc bias, and the sample integration time was 10 s. Every capacitance measurement consisted of 13 frequency sweeps (each from 100 to 1 kHz, at evenly spaced logarithmic intervals) at positive dc biases that were stepped over the desired potential range in 50 mV increments.

The equivalent circuit assumed in this work was a resistor R_{cell} (the resistance of the solution and the bulk semiconductor) in series with two parallel components, a resistor R_{sc} (the resistance to Faradaic charge transfer) and a capacitor C_{sc} (the semiconductor space-charge capacitance). The value of R_{cell} was typically 20 Ω. The value of R_{sc} at each dc potential was derived from the diameter of the circular fit of the Nyquist curve, which plots the imaginary component of the impedance, Z_{im}, vs the real component of the impedance, Z_{re}. In these differential capacitance measurements, the angular frequency ω of the excitation voltage obeyed the condition $\omega \gg (C_{sc}R_{sc})^{-1}$, and R_{cell} was therefore not included in the extraction of the C_{sc} values. The appropriate formula relating the impedance to the capacitance is then

$$C_{sc} = \frac{1 + \sqrt{1 - 4\dfrac{Z_{im}^{\,2}}{R_{sc}^{\,2}}}}{2\omega Z_{im}} \quad (6)$$

Since C_{sc} is much less than the differential capacitance of either the Helmholtz layer or the double layer, the measured differential capacitance C_{diff} was, to an excellent approximation, equal to the desired quantity C_{sc}. The C_{diff} vs E data were thus interpreted through use of the Mott−Schottky equation:[15]

$$C_{diff}^{\,-2} = \frac{2}{q\epsilon\epsilon_0 N_d A_s^{\,2}}\left(E - E_{fb} - \frac{kT}{q}\right) \quad (7)$$

where ϵ is the dielectric constant of the semiconductor (11.7 for Si), ϵ_0 is the permittivity of free space, N_d is the dopant density of the semiconductor, A_s is the area of the semiconductor electrode, and E_{fb} is the flat-band potential. Each linear regression of a $C_{diff}^{\,-2}$ vs E ("Mott−Schottky" or "M−S") plot was extrapolated to $C_{diff}^{\,-2} = 0$ and adjusted by kT/q to yield the value of E_{fb} for that measurement frequency. E_{fb} is related to the barrier height of the junction, ϕ_b, by the equation[24]

$$\phi_b = E(A/A^-) - \frac{\mathbf{E}_{cb}}{q} = E(A/A^-) - E_{fb} + \frac{kT}{q}\ln\left(\frac{N_c}{N_d}\right) \quad (8)$$

The values of $N_c = 2.8 \times 10^{19}$ cm^{-3} (ref 24) and either $N_d = 6.95 \times 10^{15}$ cm^{-3} (for the 0.74 Ω cm n-Si) or $N_d = 7.84 \times 10^{14}$ cm^{-3} (5.9 Ω cm) were used in the calculations that related ϕ_b to E_{fb}.

It should be noted that the experimental conditions described above yielded reproducible barrier height results that varied only slightly with the ac frequency and that other conditions resulted in irreproducibility or frequency dispersion in the M−S plots. Electrode areas of 0.1−0.2 cm^2 displayed more frequency dispersion than did electrode areas of 0.75−0.85 cm^2. Acceptor ion concentrations of 5 mM or less led to irreproducible barrier height results and produced $C^{-2}-E$ behavior whose slopes deviated from the predictions of eq 7.[41] Similarly, if the measuring resistor of the impedance analyzer was too low, the M−S plots were dependent on the ac signal frequency. Careful attention to all of these instrumental and cell-dependent factors was required in order to obtain the experimental behavior reported herein.

III. Results

Two separate criteria are required for a reliable rate constant evaluation in response to a changing driving force at the semiconductor/liquid junction. The interface must display ideal energetic behavior as well as ideal kinetic behavior. The junction energetics are discussed in the following section, and the results of the kinetic measurements are then presented in section III.B.

A. $C^{-2}-E$ Data for n-Si/$CH_3OH-Viologen^{2+/+}$ Contacts. Figure 2 presents typical Bode plots for two of the n-Si/CH_3OH junctions studied in this work. Figure 2a shows Bode plots obtained at two different potentials of an n-Si/$CH_3OH-\mathbf{V}^{2+/+}$ junction, while Figure 2b shows analogous data for an n-Si/$CH_3OH-\mathbf{II}^{2+/+}$ contact. For all junctions, the Bode plots were linear over at least 1 order of magnitude variation in frequency, and such behavior was observed at a variety of potentials in reverse bias. For example, in Figure 2a, the slopes of the impedance magnitude $|Z|$ vs the ac signal frequency were

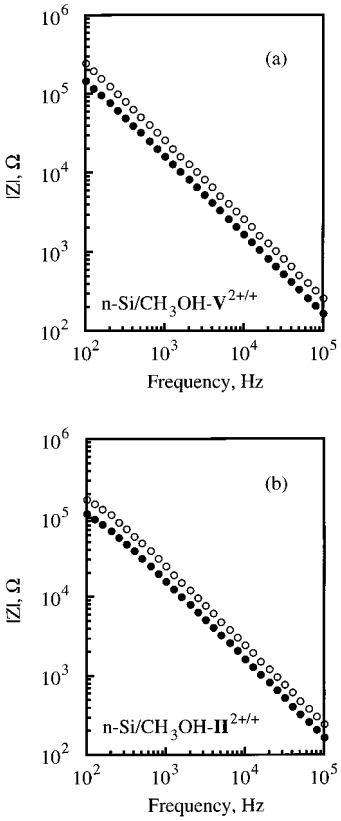

Figure 2. Representative Bode plots (impedance $|Z|$ vs frequency) for the n-Si/CH_3OH junction. (a) Bode plots for the n-Si/CH_3OH-$\mathbf{V}^{2+/+}$ interface are shown for an applied potential of +0.200 V vs $E(A/A^-)$ (●) and for an applied potential of +0.800 V vs $E(A/A^-)$ (○). In both cases, the concentrations of the redox couple were $[A] = [A^-] = 10$ mM. $E(A/A^-)$ was −0.382 V vs SCE. The n-Si electrode had a measured dopant density of 7.84×10^{14} cm^{-3} and a photographic area of 0.75 cm^2. (b) Bode plots for the n-Si/CH_3OH−$\mathbf{II}^{2+/+}$ interface for an applied potential of +0.300 V vs $E(A/A^-)$ (●) and for an applied potential of +0.800 V vs $E(A/A^-)$ (○). The concentrations of the redox couple were $[A] = [A^-] = 10$ mM. $E(A/A^-)$ was −0.518 V vs SCE. The n-Si electrode had a measured dopant density of 7.84×10^{14} cm^{-3} and a photographic area of 0.75 cm^2.

−0.998 at +0.200 V vs $E(A/A^-)$ and −1.000 at +0.800 V vs $E(A/A^-)$. The linearity and slopes of these plots indicated that the system behaved as a simple capacitive circuit element from $\approx 10^3$ to 10^5 Hz, verifying that the imaginary component $Z_{im} \approx (\omega C_{diff})^{-1}$ dominated the total impedance of the cell under such conditions.

Since the Bode plots were linear over a significant range of frequencies and potentials (Table 2), the simple equivalent circuit described in section II.C, in which $C_{diff} = C_{sc}$, was assumed to be adequate to describe the impedance behavior. If this model is correct, plots of C_{sc}^{-2} vs E should be linear and should have a slope that can be calculated from the area and dopant density of the semiconductor (eq 7). From the E_{fb} results, the position of the conduction band edge can then be calculated according to eq 8.

Figure 3 displays some representative Mott−Schottky ($C^{-2}-E$) plots for n-Si/CH_3OH−viologen$^{2+/+}$ contacts under conditions that yielded linear Bode plots. Regression of the $C^{-2}-E$ data yielded slopes that were in good agreement with those expected from the known dopant density and area of the electrodes. Moreover, the $C^{-2}-E$ slopes displayed minimal frequency dispersion. This behavior was expected because the linear Bode plots indicated that the measured differential capacitance was essentially independent of the measurement frequency.

The intercepts on the x-axis of $C^{-2}-E$ plots yielded the desired energetic data for the junctions of concern. For a given solid/liquid contact, the extrapolated intercepts of the data collected at various measurement frequencies were generally within 10−20 mV of each other (Table 3). Because errors in the value of the conduction band edge energy translate exponentially into errors in the calculated rate constant (eqs 3 and 8), significant effort was devoted to obtaining reliable statistical measures of the mean and standard deviation of the value of $\mathbf{E}_{cb}$ for each system. Each value was obtained by first averaging, for each junction, the barrier height values that were computed from $C^{-2}-E$ plots obtained at six different measurement frequencies. These frequencies were chosen to represent the extent of ϕ_b variation over the relevant Bode plot range. The ϕ_b averages of six to eight junctions of nominally identical solution compositions and Si electrodes were further combined to yield an average and a standard deviation for the interface of concern. These data are also summarized in Table 3. We believe that the reported standard deviations for determination of $\mathbf{E}_{cb}$, which are generally <20 meV, represent reliable estimates of the random errors involved in our $C^{-2}-E$ analysis of $\mathbf{E}_{cb}$ for each contact.

Since validation of the rate law of eq 2 generally involved changing the concentration of redox acceptor while holding the concentration of the redox donor constant, it was important to ensure that the band edge positions were fixed as $E(A/A^-)$ varied. Otherwise, different rate constants would be calculated at different acceptor concentrations, and interpretation of the kinetic data would be problematic. One method to evaluate whether $\mathbf{E}_{cb}/q$ was fixed vs a standard reference potential was to investigate whether the observed barrier height for a given redox system changed in response to changes in $E(A/A^-)$. For a fixed value of $\mathbf{E}_{cb}$, ϕ_b should respond to the variation in $E(A/A^-)$ induced by changing the concentration of donors or of acceptors in the solution phase. As outlined in Table 3, such behavior was generally observed, within experimental error, for each n-Si/CH_3OH−viologen$^{2+/+}$ contact studied in this work.

An alternate, and arguably more statistically meaningful, approach to validating that $\mathbf{E}_{cb}/q$ was fixed vs an absolute reference potential is to combine the entire collection of ϕ_b vs $E(A/A^-)$ data for all redox systems investigated in this work and to plot the entire data set on a single graph. If the band edge position were fixed and no Fermi level pinning[15] were to occur over the potential range of interest, then ϕ_b should increase linearly with $E(A/A^-)$ with a slope of unity, and this plot should yield a single, fixed value for the conduction band edge energy for the entire range of measurements. These data have been compiled in Figure 4. The plot clearly shows a linear dependence of ϕ_b on $E(A/A^-)$ for the entire set of n-Si/CH_3OH−viologen$^{2+/+}$ contacts. A linear-regression analysis of ϕ_b against $\mathbf{E}(A/A^-)$ yielded a slope of 0.984 ± 0.044 and a correlation coefficient of 0.988. The x-intercept produced a value for $\mathbf{E}_{cb}/q$ of −0.920 ± 0.044 V vs SCE for these sets of Si/CH_3OH contacts, which was taken to be a reliable mean determination of E_{cb}/q for the junctions studied in this work.

B. $J-E$ Behavior for n-Si/CH_3OH−Viologen$^{2+/+}$ Contacts. All of the n-Si/CH_3OH−viologen$^{2+/+}$ contacts exhibited rectifying $J-E$ behavior, producing a limiting value for the anodic current density and an approximately exponential increase in the cathodic current density as E was made more negative. Figure 5 displays the as-collected $J-E$ data for an n-Si/CH_3OH junction in contact with three typical redox systems, $\mathbf{III}^{2+/+}$, $\mathbf{V}^{2+/+}$, and $\mathbf{VII}^{2+/+}$. For each system, the figure also displays the $J-E$ behavior that was measured at a

TABLE 2: Impedance Data for n-Si/CH_3OH Interfaces[b]

I$^{2+/+}$

potential, V vs $E(A/A^-)$	slope of Bode plot	average C, 10^{-9} F[a]	potential, V vs $E(A/A^-)$	slope of Bode plot	average C, 10^{-9} F[a]
+0.400	−0.987	8.47 ± 0.09	+0.750	−0.994	6.32 ± 0.02
+0.450	−0.992	8.00 ± 0.04	+0.800	−0.994	6.14 ± 0.02
+0.500	−0.994	7.61 ± 0.03	+0.850	−0.994	5.97 ± 0.02
+0.550	−0.994	7.29 ± 0.03	+0.900	−0.994	5.82 ± 0.02
+0.600	−0.994	7.00 ± 0.03	+0.950	−0.994	5.67 ± 0.02
+0.650	−0.994	6.75 ± 0.02	+1.000	−0.994	5.54 ± 0.02
+0.700	−0.994	6.52 ± 0.02			

II$^{2+/+}$

potential, V vs $E(A/A^-)$	slope of Bode plot	average C, 10^{-9} F[a]	potential, V vs $E(A/A^-)$	slope of Bode plot	average C, 10^{-9} F[a]
+0.300	−0.996	9.01 ± 0.03	+0.600	−0.999	6.79 ± 0.01
+0.350	−0.998	8.46 ± 0.01	+0.650	−0.999	6.57 ± 0.01
+0.400	−0.999	8.02 ± 0.01	+0.700	−0.999	6.37 ± 0.01
+0.450	−0.999	7.65 ± 0.01	+0.750	−0.999	6.19 ± 0.01
+0.500	−0.999	7.33 ± 0.01	+0.800	−0.999	6.02 ± 0.01
+0.550	−0.999	7.04 ± 0.01			

III$^{2+/+}$

potential, V vs $E(A/A^-)$	slope of Bode plot	average C, 10^{-9} F[a]	potential, V vs $E(A/A^-)$	slope of Bode plot	average C, 10^{-9} F[a]
+0.300	−1.002	9.46 ± 0.09	+0.600	−1.001	7.58 ± 0.07
+0.350	−1.003	9.03 ± 0.09	+0.650	−1.001	7.37 ± 0.06
+0.400	−1.003	8.67 ± 0.09	+0.700	−1.001	7.17 ± 0.06
+0.450	−1.003	8.35 ± 0.08	+0.750	−1.001	6.99 ± 0.06
+0.500	−1.002	8.07 ± 0.08	+0.800	−1.000	6.82 ± 0.06
+0.550	−1.002	7.81 ± 0.07			

IV$^{2+/+}$

potential, V vs $E(A/A^-)$	slope of Bode plot	average C, 10^{-8} F[a]	potential, V vs $E(A/A^-)$	slope of Bode plot	average C, 10^{-8} F[a]
+0.200	−0.992	2.48 ± 0.01	+0.550	−0.993	1.85 ± 0.01
+0.250	−0.994	2.35 ± 0.01	+0.600	−0.992	1.79 ± 0.01
+0.300	−0.994	2.23 ± 0.01	+0.650	−0.992	1.75 ± 0.01
+0.350	−0.994	2.14 ± 0.01	+0.700	−0.991	1.70 ± 0.01
+0.400	−0.993	2.05 ± 0.01	+0.750	−0.991	1.66 ± 0.01
+0.450	−0.993	1.97 ± 0.01	+0.800	−0.991	1.62 ± 0.01
+0.500	−0.993	1.91 ± 0.01			

V$^{2+/+}$

potential, V vs $E(A/A^-)$	slope of Bode plot	average C, 10^{-9} F[a]	potential, V vs $E(A/A^-)$	slope of Bode plot	average C, 10^{-9} F[a]
+0.200	−0.998	9.55 ± 0.03	+0.550	−0.999	7.02 ± 0.01
+0.250	−0.999	9.01 ± 0.02	+0.600	−0.999	6.81 ± 0.01
+0.300	−0.999	8.55 ± 0.01	+0.650	−1.000	6.62 ± 0.01
+0.350	−0.999	8.16 ± 0.01	+0.700	−0.999	6.45 ± 0.01
+0.400	−0.999	7.82 ± 0.01	+0.750	−1.000	6.27 ± 0.01
+0.450	−0.999	7.52 ± 0.01	+0.800	−1.000	6.12 ± 0.01
+0.500	−0.999	7.26 ± 0.01			

VI$^{2+/+}$

potential, V vs $E(A/A^-)$	slope of Bode plot	average C, 10^{-9} F[a]	potential, V vs $E(A/A^-)$	slope of Bode plot	average C, 10^{-9} F[a]
+0.200	−1.004	9.31 ± 0.08	+0.550	−1.004	7.09 ± 0.06
+0.250	−1.004	8.85 ± 0.07	+0.600	−1.004	6.90 ± 0.05
+0.300	−1.004	8.45 ± 0.07	+0.650	−1.004	6.72 ± 0.05
+0.350	−1.004	8.11 ± 0.07	+0.700	−1.004	6.56 ± 0.05
+0.400	−1.004	7.81 ± 0.06	+0.750	−1.003	6.41 ± 0.05
+0.450	−1.004	7.55 ± 0.06	+0.800	−1.003	6.27 ± 0.05
+0.500	−1.004	7.31 ± 0.06			

VII$^{2+/+}$

potential, V vs $E(A/A^-)$	slope of Bode plot	average C, 10^{-9} F[a]	potential, V vs $E(A/A^-)$	slope of Bode plot	average C, 10^{-9} F[a]
+0.000	−1.006	9.87 ± 0.12	+0.350	−1.006	7.22 ± 0.08
+0.050	−1.006	9.30 ± 0.11	+0.400	−1.006	7.00 ± 0.08
+0.100	−1.006	8.83 ± 0.11	+0.450	−1.006	6.79 ± 0.07
+0.150	−1.006	8.42 ± 0.10	+0.500	−1.005	6.61 ± 0.07
+0.200	−1.006	8.07 ± 0.09	+0.550	−1.005	6.43 ± 0.07
+0.250	−1.006	7.75 ± 0.09	+0.600	−1.005	6.28 ± 0.06
+0.300	−1.006	7.47 ± 0.08			

[a] Standard deviations are reported. [b] For all data, $[A] = [A^-] = 10$ mM. The upper limit of the ac frequency range for each n-Si/CH_3OH interface was 100.0 kHz. Various lower limits of the frequency range were used: **I**, 6.3 kHz; **II**−**IV**, 4.0 kHz; **V**−**VII**, 2.5 kHz. In each decade of ac frequency, 10 individual frequencies, which were equally spaced on a logarithmic scale, comprised the data set. In no case was the correlation coefficient for the slope of the Bode plot less than 1.0000. For these impedance measurements, the areas of the relevant n-Si electrodes were as follows: **I**, 0.75 cm^2; **II**, 0.75 cm^2; **III**, 0.81 cm^2; **IV**, 0.78 cm^2; **V**, 0.83 cm^2; **VI**, 0.86 cm^2; **VII**, 0.83 cm^2. The data for the n-Si/CH_3OH-**IV**$^{2+/+}$ interface were obtained using a semiconductor electrode of $N_d = 6.95 \times 10^{15}$ cm^{-3}, and the data for all other n-Si/CH_3OH contacts were obtained using semiconductor electrodes of $N_d = 7.84 \times 10^{14}$ cm^{-3}.

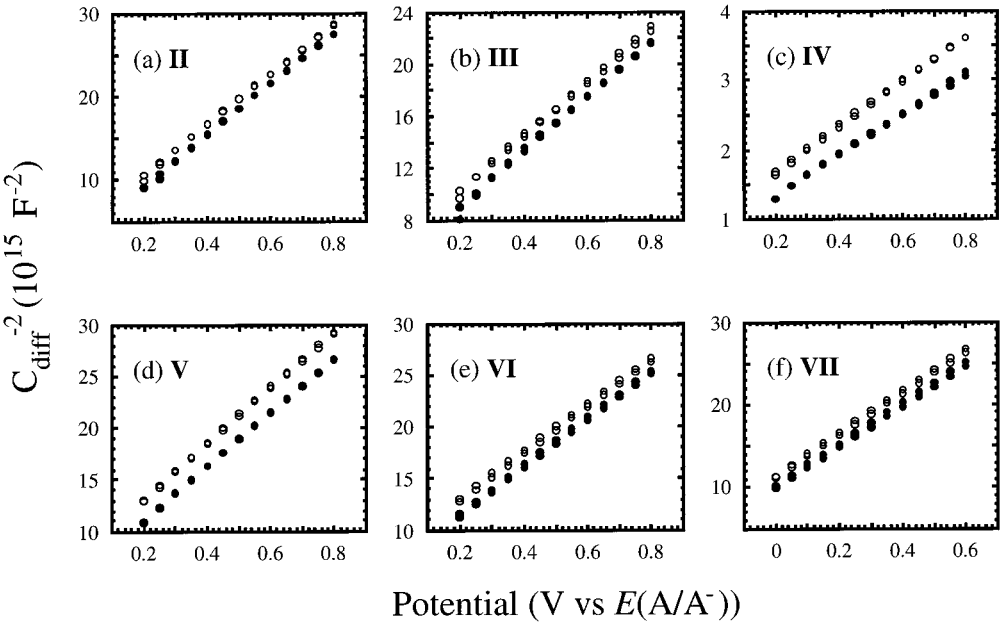

Figure 3. Mott−Schottky plots for compounds **II**−**VII**, each illustrating the shift in electric field at different [A] and constant [A$^-$]. The donor concentration [A$^-$] was always 10 mM. The filled circles in all plots represent data for [A] = 10 mM, while the open circles represent data for [A] = 100 mM in plots a−e and [A] = 85 mM in plot f. In plots a, b, d−f, the N_d measured from four-point probe techniques was 7.84×10^{14} cm^{-3}, whereas in plot c, the measured N_d was 6.95×10^{15} cm^{-3}. Areas of the n-Si electrodes were 0.75−0.85 cm^2. The M−S results used the average of six frequencies equally spaced logarithmically; for clarity, only the data of the upper and lower limits of each frequency range are displayed. The relevant frequency ranges are given in Tables 2 and 3. (a) The average shift in ϕ_b was 54 mV. (b) $\Delta\phi_b$ = 71 mV. (c) $\Delta\phi_b$ = 58 mV. (d) $\Delta\phi_b$ = 63 mV. (e) $\Delta\phi_b$ = 80 mV. (f) $\Delta\phi_b$ = 40 mV.

TABLE 3: Barrier Height Results for n-Si/CH_3OH Interfaces[g]

	$\mathbf{I}^{2+/+}$		$\mathbf{II}^{2+/+}$		$\mathbf{III}^{2+/+}$		$\mathbf{IV}^{2+/+}$		$\mathbf{V}^{2+/+}$		$\mathbf{VI}^{2+/+}$		$\mathbf{VII}^{2+/+}$	
frequency, kHz	ϕ_b,[a] V	pred N_d,[b] 10^{14} cm^{-3}	ϕ_b,[a] V	pred N_d,[b] 10^{14} cm^{-3}	ϕ_b,[a] V	pred N_d,[b] 10^{15} cm^{-3}	ϕ_b,[a] V	pred N_d,[b] 10^{15} cm^{-3}	ϕ_b,[a] V	pred N_d,[b] 10^{14} cm^{-3}	ϕ_b,[a] V	pred N_d,[b] 10^{14} cm^{-3}	ϕ_b,[a] V	pred N_d,[b] 10^{14} cm^{-3}
100.00	0.353	6.75	0.406	6.96	0.529	1.00	0.472	5.67	0.518	8.08	0.588	9.14	0.699	8.60
79.433	0.357	6.77	0.406	6.97	0.533	1.00	0.483	5.72	0.519	8.10	0.590	9.17	0.697	8.61
63.096	0.357	6.80	0.407	6.95	0.535	1.00	0.491	5.73	0.519	8.09	0.592	9.14	0.698	8.57
50.119	0.356	6.79	0.407	6.94	0.537	1.01	0.494	5.75	0.520	8.09	0.594	9.16	0.700	8.54
39.811	0.357	6.82	0.407	6.94	0.540	1.04	0.490	5.72	0.520	8.07	0.599	9.25	0.701	8.42
31.623	0.355	6.82	0.407	6.93	0.539	1.07	0.486	5.69	0.520	8.05	0.605	9.33	0.704	8.29
25.119	0.355	6.84	0.406	6.91	0.537	1.05	0.485	5.70	0.519	8.04	0.604	9.23	0.706	8.28
19.953	0.355	6.85	0.406	6.90	0.537	1.03	0.486	5.72	0.520	8.04	0.602	9.12	0.707	8.30
15.849	0.354	6.86	0.405	6.90	0.539	1.02	0.491	5.77	0.520	8.04	0.600	9.04	0.707	8.28
12.589	0.351	6.85	0.404	6.89	0.543	1.02	0.496	5.83	0.520	8.05	0.601	8.98	0.707	8.25
10.000	0.349	6.85	0.404	6.89	0.544	1.02	0.501	5.89	0.520	8.06	0.599	8.92	0.707	8.21
7.9433	0.345	6.83	0.403	6.89	0.548	1.02	0.505	5.94	0.519	8.05	0.599	8.90	0.707	8.20
6.3906	0.342	6.81	0.401	6.88	0.554	1.02	0.508	6.00	0.518	8.05	0.602	8.93	0.706	8.20
5.0019			0.400	6.88	0.557	1.03	0.510	6.04	0.518	8.05	0.602	8.95	0.706	8.22
3.9811			0.398	6.88	0.561	1.04	0.510	6.07	0.518	8.06	0.602	9.01	0.706	8.29
3.1623									0.515	8.04	0.601	9.07	0.707	8.38
2.5119									0.513	8.03	0.601	9.14	0.705	8.44
avg ϕ_b, V, one electrode[c] [A] = 10 mM	0.353 ± 0.005		0.404 ± 0.003		0.542 ± 0.009		0.494 ± 0.011		0.519 ± 0.002		0.599 ± 0.005		0.704 ± 0.004	
avg. ϕ_b, V, all electrodes[d] [A] = 10 mM	0.331 ± 0.015		0.396 ± 0.014		0.508 ± 0.021		0.491 ± 0.012		0.509 ± 0.015		0.613 ± 0.020		0.695 ± 0.018	
avg ϕ_b, V, all electrodes [A] = 100 mM	*e*		0.434 ± 0.018		0.608 ± 0.018		0.541 ± 0.021		0.567 ± 0.012		0.690 ± 0.008		0.758 ± 0.012 [f]	

[a] Data from one representative contact between a single n-Si electrode and the specified redox couple. The average ϕ_b from these data is listed in the row labeled "one electrode". The n-Si electrode areas and dopant densities ($N_d = 6.95 \times 10^{15}$ cm^{-3} for the $\mathbf{IV}^{2+/+}$ interface, 7.84×10^{14} cm^{-3} for all other interfaces) are identical with those specified in Table 2. [b] Predicted N_d values are derived from the slopes of the $C^{-2}-E$ plots. [c] Standard deviations are reported with the average values. [d] Average values of ϕ_b over all electrodes, representing the results from six to eight separate n-Si/CH_3OH contacts. Each individual result was itself an average of ϕ_b values obtained at six different ac measurement frequencies, selected to indicate the extent of ϕ_b variation over the pertinent frequency range. [e] The second-order kinetic rate law was tested by increasing the concentrations to [A] = [A$^-$] = 30 mM. [f] [A] = 85 mM. [g] [A$^-$] = 10 mM for all data shown here. The potential limits for the $C^{-2}-E$ measurements for each redox compound are given in Table 2, and in no case was the correlation coefficient for the slope of the $C^{-2}-E$ plot less than 0.9996.

Pt electrode of similar area and in nominally the same cell configuration as that of the Si electrode. Clearly, the current density at the Si electrode was limited by kinetics and not by mass transport because the current density at each potential of the Pt electrode was significantly larger than that observed at the Si electrode surface.

Figure 6 displays the $J-E$ data, in the form of $\ln|J|$ vs E_{corr}, following correction for concentration and series resistance overpotentials. The protocols used to perform these corrections are described in the Experimental Section and are in accord with conventional electrochemical treatments of these effects.[18] These corrections were required because the nonaqueous solvent

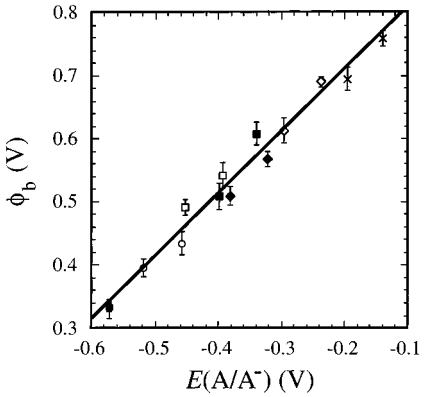

Figure 4. Plot of the barrier height vs the Nernstian solution potential. Each of the compounds **I**−**VII** contributed two ϕ_b points, one at [A] = [A$^-$] = 10 mM and one at either [A] = [A$^-$] = 30 mM (**I**) or [A] > [A$^-$] = 10 mM (**II**−**VII**). Each compound is represented by the following symbols: **I** (●); **II** (○); **III** (■); **IV** (□); **V** (◆); **VI** (◇); **VII** (×). The linear regression slope was 0.984 ± 0.044, and the correlation coefficient was 0.988.

had a significantly higher cell resistance than the aqueous solutions used in previous kinetic studies.[2,5] In addition, limitations on the concentration of redox species due to solubility considerations imposed nonnegligible mass-transport overpotential corrections at the highest current densities of interest. The corrected $J-E$ data yielded excellent linearity in $\ln|J|$ vs E_{corr} plots, indicating adherence to the diode-like behavior expected for a semiconductor/liquid contact. The diode quality factors, γ, which describe the ratio of the experimentally measured slope of $\ln|J|$ vs E to theoretical expectations, were not precisely unity but were generally close to the predicted value of 1.0; mean values of γ ranged from 1.1 to 1.4 for the various junctions of interest (Table 4). The diode quality factor can be interpreted as the reaction order of the interfacial kinetics in the surface electron concentration, with a quality factor of 1.0 indicating a strict first-order kinetic dependence on n_s, as predicted by eq 2.

Figure 6 also depicts the change in $\ln|J| - E_{corr}$ data for six viologen redox systems in response to variation in the concentration of the acceptor species A. If the rate law of eq 2 were obeyed, increasing the acceptor concentration by a factor of 10 should decrease the value of E_{corr} vs a fixed reference, such as SCE, by $(kT/q)(\ln 10) = 59$ mV, to obtain a given current density. This behavior was generally observed for all of the junctions investigated in this work, with the data for all systems summarized in Table 4.

Rate constant data were computed by dividing the current density by the quantity $\{qn_s[A]\}$. The value of [A] was taken to be the same as its value in the bulk of the solution because the Frumkin-like double-layer corrections that relate the concentration of redox species at the edge of the outer Helmholtz plane to the concentration of redox species in the bulk of the solution are negligible for a semiconductor electrode under depletion conditions.[33] The value of n_s was computed according to eqs 3 and 8 using the value of ϕ_b obtained from analysis of the $C^{-2}-E$ data for the specific junction of concern. For example, for one particular n-Si/CH_3OH−**IV**$^{2+/+}$ cell, $J = -2.88 \times 10^{-4}$ A cm^{-2} at $E_{corr} = -0.087$ V vs E(A/A$^-$) with [A] = 10 mM. The value of ϕ_b was determined as 0.477 V, so eqs 3 and 8 yielded $n_s = 7.19 \times 10^{12}$ cm^{-3} at $E_{corr} = -0.087$ V vs E(A/A$^-$). Substitution of these values into the rate law of eq 2 produces $k_{et} = 4.2 \times 10^{-17}$ cm^4 s^{-1} for this specific measurement. For a given n-Si/CH_3OH interface with compounds **II**−**VII**, 12−16 individual rate constant determinations, each using the J and ϕ_b measurements from one particular electrode−solution combination, resulted in an average k_{et} and an associated standard deviation for that system.

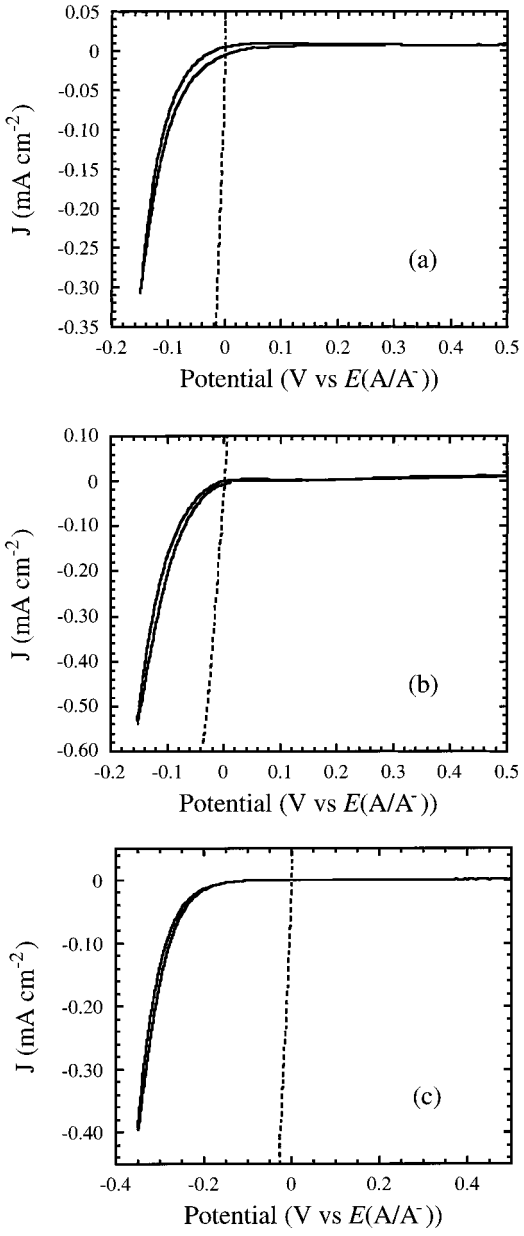

Figure 5. Representative current density−potential ($J-E$) behavior for electrodes in contact with CH_3OH−bipyridinium$^{2+/+}$ solutions. The solid line represents the J at an n-Si working electrode, while the dashed line depicts the J at a Pt working electrode of similar geometry (1.31 cm^2). The data have not been corrected for concentration overpotentials or for cell resistance. For each set of $J-E$ data shown, the redox solution consisted of [A] = [A$^-$] = 10 mM. The dopant density of the n-Si was 7.84×10^{14} cm^{-3} for all three $J-E$ curves. (a) The redox couple was **III**$^{2+/+}$, and the n-Si electrode area was 0.81 cm^2. The solution potential E(A/A$^-$) was −0.399 V vs SCE. (b) The redox couple was **V**$^{2+/+}$. The n-Si electrode area was 0.83 cm^2. E(A/A$^-$) was −0.382 V vs SCE. (c) The redox couple was **VII**$^{2+/+}$. The n-Si electrode area was 0.83 cm^2. E(A/A$^-$) was −0.195 V vs SCE.

The diode quality factors of 1.1−1.4 introduced two ambiguities into the data analysis. The γ values greater than unity might suggest a recombination mechanism other than electron transfer from the semiconductor conduction band to the solution acceptor, since J changed with E_{corr} to a smaller extent than described by eqs 2 and 3. However, the possibility of surface-state mediation is contradicted by the dependence of J on both redox concentration and applied potential. The corrections of E for overpotential and resistance effects may have introduced

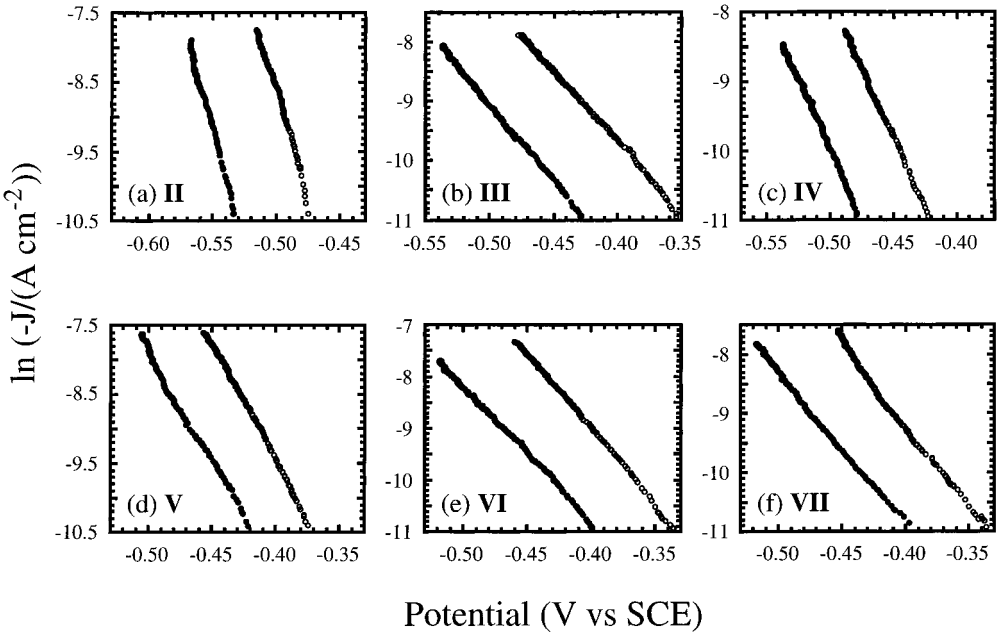

Figure 6. Dark $J-E_{corr}$ characteristics for compounds **II**−**VII**, each showing the shift as [A] was increased and [A^-] held constant. In each plot, the curve on the left is the $J-E$ response at [A] = [A^-] = 10 mM, while the curve to the right is that at [A] = 100 mM (85 mM for part f) and [A^-] = 10 mM. For clarity, the potential is referenced to SCE. As detailed in the text, a 10-fold higher [A] with fixed [A^-] should shift the Nernstian potential by +59 mV, increase the barrier height by 59 mV, and decrease the potential vs SCE that is needed to obtain a given current density by 59 mV. The cells described in parts a−f correspond to the cells shown in parts a−f of Figure 3.

TABLE 4: Current Density−Potential Data for n-Si/CH_3OH Interfaces[d]

redox compound	diode quality factor	current density[a] (mA cm^{-2})	E shift with [A][b] (mV vs SCE)
II	1.37	−0.373	52
III	1.44	−0.305	68
IV	1.04	−0.209	52
V	1.16	−0.489	51
VI	1.34	−0.453	73
VII	1.49	−0.397	69[c]

[a] The maximum cathodic J for which data were analyzed for each n-Si/CH_3OH junction in cells with [A] = [A^-] = 10 mM. This current density is also the value at which the dependence of J on acceptor concentration was assessed. [b] For each specified current density, the shift in potential (vs SCE) as [A] was changed from 10 to 100 mM, while [A^-] was constant at 10 mM. In the case of fixed band edges, the expected shift for a 10-fold increase in [A] is 59 mV. [c] Since [A] was increased from 10 to 85 mM in this particular experiment, the expected shift in potential vs SCE is 55 mV. [d] The diode quality factors represent the mean of the two (ln J)$-E_{corr}$ curves illustrated in Figure 6.

a residual systematic error into the $J-E_{corr}$ curves. The second issue concerns the choice of $J-E_{corr}$ points used in each k_{et} calculation. If $\gamma > 1$, the k_{et} calculated from eqs 2 and 3 would decrease with larger J and E_{corr} values. In this work, any artificial variations in k_{et} were minimized by choosing similar current densities (−(2 to 5) × 10^{-4} A cm^{-2}) for the rate constant calculations for compounds **II**−**VII**. In addition, the maximum J and E_{corr} of each interface were used because at higher forward bias, the cathodic recombination pathways that have $\gamma = 1$ prevail over those that have $\gamma > 1$.

For the redox couple with the most negative redox potential, $\mathbf{I}^{2+/+}$, a different approach was required to evaluate the interfacial charge-transfer kinetics. The low barrier height of this system produced a relatively high exchange current density and therefore resulted in significant interfacial currents at relatively small forward bias potentials relative to E(A/A^-). In fact, the cathodic current densities for n-Si/$CH_3OH-\mathbf{I}^{2+/+}$ contacts were sufficiently large that mass-transport limits constrained the potential range available for study. For these systems, the interfacial kinetics were instead evaluated through measurement of the anodic saturation current density, J_0. The anodic saturation current density reflects the rate of electron movement from the donor species in solution into the conduction band of the semiconductor. Because the full diode equation is[24]

$$J = -J_0[\exp(-qE_{corr}/(kT)) - 1] \quad (9)$$

the value of J_0 at positive potentials can be directly related to the desired interfacial rate constant without evaluating a plot of ln|J| vs E_{corr} at negative potentials.

Although the saturation current density for high-barrier-height systems is notoriously sensitive to the presence of surface defects,[15] the low barrier height of n-Si/CH_3OH junctions with the redox species **I** and **II** produced a sufficiently large saturation current density that leakage currents were insignificant. This behavior allowed estimation of the rate constant from an analysis of the anodic portion of the $J-E$ data. To verify this approach, the rate constant for compound **II** was determined from both the anodic and cathodic portions of $J-E$ plots. A k_{et} of 2.7 × 10^{-17} cm^4 s^{-1} was computed for an n-Si/$CH_3OH-\mathbf{II}^{2+/+}$ contact from the cathodic $J-E$ data and a k_{et} of 1.7 × 10^{-17} cm^4 s^{-1} was obtained from the anodic J_0 value.

For n-Si/$CH_3OH-\mathbf{I}^{2+/+}$ contacts, the kinetics scaled with acceptor concentration. For example, the exchange current density of an n-Si/CH_3OH contact was 2.67 × 10^{-4} A cm^{-2} in a solution of [$\mathbf{I}^{2+}$] = [$\mathbf{I}^{+}$] = 10 mM but was 6.61 × 10^{-4} A cm^{-2} in a more concentrated solution of [$\mathbf{I}^{2+}$] = [$\mathbf{I}^{+}$] = 30 mM (Figure 7). With the measured barrier heights of 0.331 V for the 10 mM solution and 0.334 V for the 30 mM solution, these J_0 data produced rate constants of 3.9 × 10^{-18} and 3.6 × 10^{-18} cm^4 s^{-1}, respectively. To ensure that the J_0 values were not limited by mass transport of donors to the electrode, the anodic current density was measured for a Pt electrode in nominally the same configuration as the Si working electrode. The limiting current densities at a Pt foil of 1.3 × 10^{-3} A cm^{-2} in the dilute solution and 3.0 × 10^{-3} A cm^{-2} in the concentrated solution were significantly in excess of the anodic saturation current

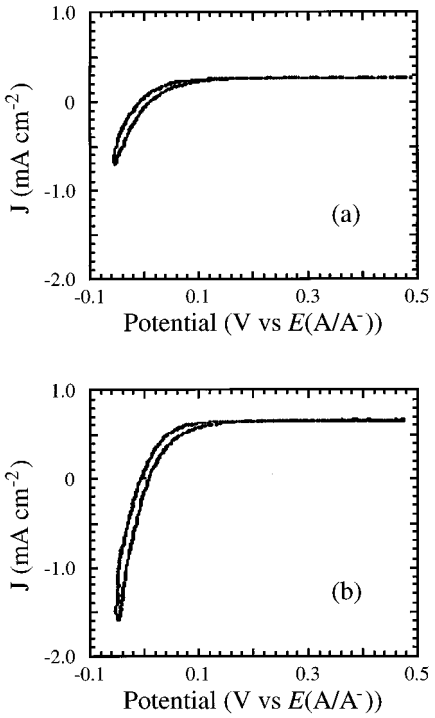

Figure 7. Dark $J-E$ properties for compound **I** at different total concentrations of redox species in solution. $E(A/A^-)$ was -0.572 V vs SCE in both cases. The n-Si electrode had a measured N_d of 7.84×10^{14} cm^{-3} and an area of 0.75 cm^2. (a) At $[A] = [A^-] = 10$ mM, the J_0 observed at $+0.450$ V vs $E(A/A^-)$ was 2.67×10^{-4} A cm^{-2}. (b) At $[A] = [A^-] = 30$ mM, the J_0 at $+0.450$ V vs $E(A/A^-)$ was 6.61×10^{-4} A cm^{-2}.

densities at the n-Si contacts, so no mass-transport corrections were required in the analysis of the Si electrode data obtained under these conditions.

C. Trend in k_{et} for n-Si/CH$_3$OH−Viologen$^{2+/+}$ Contacts. Figure 8a presents a semilogarithmic plot of k_{et} vs the standard driving force for interfacial electron transfer, $\Delta G^{\circ\prime}$. This latter quantity is the driving force for an electron at the surface transferring to an acceptor under standard conditions and is thus given as $\mathbf{E}_{cb} - qE^{\circ\prime}(A/A^-)$. The driving force for each n-Si/CH$_3$OH−viologen$^{2+/+}$ contact was determined from measurements of the barrier height when $E(A/A^-) = E^{\circ\prime}(A/A^-)$, i.e., specifically in this work when $[A] = [A^-] = 10$ mM.

The data were fit to a classical version of the Marcus theory, which has the form

$$k_{et} = k_{et,max} \exp\left\{\frac{-(\Delta G^{\circ\prime} + \lambda)^2}{4\lambda kT}\right\} \qquad (10)$$

where λ is the reorganization energy at the interface. In this analysis, $k_{et,max}$ and λ were both floating parameters. The ensuing fit, with all experimental data points weighted equally, yielded $k_{et,max} = (6.4 \pm 1.7) \times 10^{-17}$ cm^4 s^{-1} and $\lambda = 0.67 \pm 0.12$ eV. A slightly more visually satisfying fit to the available data, shown in Figure 8b, was obtained by increasing λ to 0.75 eV, resulting in $k_{et,max} = 6.6 \times 10^{-17}$ cm^4 s^{-1}. This fit agreed more closely with the data points at lower driving force, which are fewer in number and thus weighted less than those at higher driving force in a purely statistical analysis of this specific data set. Other λ and $k_{et,max}$ combinations did not describe the experimental data as satisfactorily (Figure 8c). When λ was constrained at 0.5 eV, $k_{et,max} = 4.6 \times 10^{-17}$ cm^4 s^{-1} was obtained as the best fit to the data, but this fit produced a significant discrepancy in the value of k_{et} for the n-Si/CH$_3$OH−**I**$^{2+/+}$ junction. When $k_{et,max}$ was constrained to 1×10^{-14} cm^4 s^{-1}, the fit deviated considerably from the k_{et} data of the n-Si/CH$_3$OH−**II**$^{2+/+}$ and the n-Si/CH$_3$OH−**VII**$^{2+/+}$ contacts. Furthermore, the constraint of $k_{et,max}$ to 1×10^{-14} cm^4 s^{-1} forced λ to be 1.4 eV, which is an unrealistically large value for the reorganization energy for this system (vide infra).

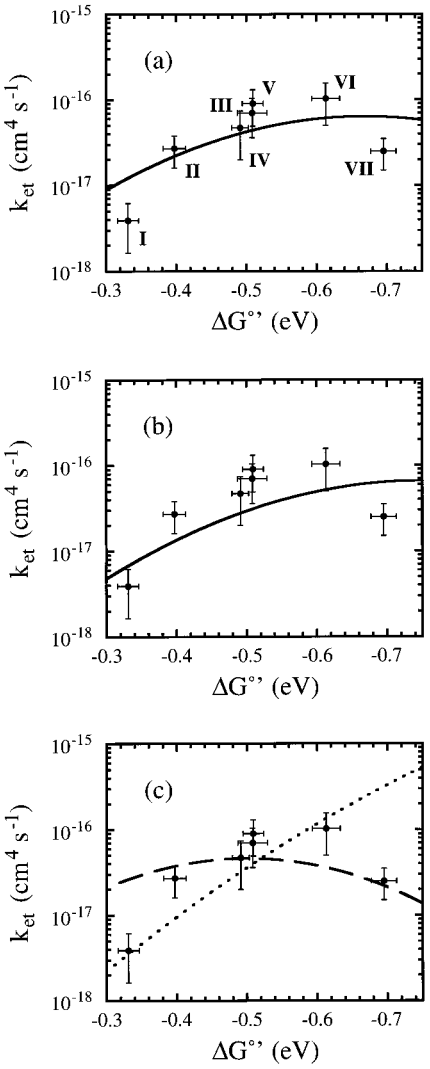

Figure 8. Plots of the electron-transfer rate constant as a function of the driving force for charge transfer. The $\Delta G^{\circ\prime}$ values were taken to be the barrier heights measured at $[A] = [A^-] = 10$ mM. The error in $\Delta G^{\circ\prime}$ was the standard deviation of ϕ_b measured at these concentrations, while the error in k_{et} was the standard deviation of 12−16 rate constant determinations for each interface. (a) When both the maximum electron-transfer rate constant and the reorganization energy were floated, the fitted parabolic curve had parameters of $k_{et,max} = (6.4 \pm 1.7) \times 10^{-17}$ cm^4 s^{-1} and $\lambda = 0.67 \pm 0.12$ eV. (b) A slightly more visually satisfying fit was obtained by using parameters of $k_{et,max} = 6.6 \times 10^{-17}$ cm^4 s^{-1} and $\lambda = 0.75$ eV. (c) When λ was fixed at 0.50 eV, the best-fit $k_{et,max}$ was 4.6×10^{-17} cm^4 s^{-1} (dashed line). When $k_{et,max}$ was fixed at 1×10^{-14} cm^4 s^{-1}, the best-fit λ was 1.4 eV (dotted line).

IV. Discussion

A. Energetic Behavior of n-Si/CH$_3$OH−Viologen$^{2+/+}$ Contacts. A striking feature of the results presented above is the nearly ideal energetic behavior of n-Si/CH$_3$OH−viologen$^{2+/+}$ contacts. Prior studies on small-bandgap semiconductors in general, and on Si electrodes in particular, have reported nonideal energetic behavior in contact with nonaqueous solvents,[8,9,42,43] although later work demonstrated that the photovoltage of Si/liquid contacts could respond almost ideally to $E(A/A^-)$.[14,44] Moreover, frequency dispersion in the differential

capacitance measurements of some semiconductor/liquid interfaces has hindered the straightforward energetic characterization of these systems.[45−49] In our work, careful control over experimental variables (e.g., etching procedures, counter electrode size, cell geometry, the perimeter/area ratio of the semiconductor electrode, etc.) led to behavior in which the Mott−Schottky plots of n-Si/CH_3OH contacts showed small frequency dispersions and displayed slopes that agreed well with theoretical expectations. The energetic parameters derived from these M−S measurements revealed that the band edge positions of the n-Si/CH_3OH contacts remained fixed to within ≈40 mV while the Nernstian potential of the solution was changed by over 400 mV (Figure 4), underscoring the lack of surface-state charging that is displayed by this system.

An upper limit on the surface state capacity for this system can be estimated from the ϕ_b vs $E(A/A^-)$ behavior of Figure 4. Assuming a differential capacitance of the Helmholtz layer of 10 μF cm^{-2} and a double layer thickness of 3 Å, 10^{12} surface states cm^{-2} (N_{ss}) would be sufficient to pin the Fermi level completely if such states were charged or discharged over the potential range of interest.[8] Within this framework, the linearity of the data of Figure 4 implies an upper bound on N_{ss} of $<10^{11}$ cm^{-2} for these systems. This low electrical defect density, which corresponds to less than 1 electrical defect per 10^4 surface atoms, attests to the high degree of electrical perfection that can be attained from small-bandgap semiconductors in carefully controlled solid/liquid junctions.

B. Kinetic Behavior of n-Si/CH_3OH−Viologen$^{2+/+}$ Contacts. A second striking feature of the n-Si/CH_3OH−viologen$^{2+/+}$ contacts is their $J-E$ behavior. Prior studies of semiconductor/liquid contacts have not observed kinetic behavior in accord with the rate law of eq 2 but have instead observed no dependence of the interfacial current density on the concentration of acceptor species in the solution phase.[4,7,14] This lack of adherence to the expected rate law of eq 2 has thwarted routine investigation of charge-transfer kinetics at semiconductor/liquid contacts, although a linear dependence of J on [A] has been observed in a few systems.[2,5,6,50] The n-Si/CH_3OH−viologen$^{2+/+}$ interfaces described in this paper display kinetics that are first-order in the acceptor concentration and first-order in the concentration of electrons at the semiconductor surface, thereby allowing k_{et} to be extracted from a simple arithmetic analysis of the current density−potential data of such systems.

The $J-E$ behavior establishes an even more strict upper limit on N_{ss} than does the $C^{-2}-E$ behavior. Including surface-state capture as an intermediate pathway for electron transfer from the semiconductor to the acceptor in solution (Scheme 3) produces the following rate law:

$$\text{rate} = k_{et}[A]n_s + k_{sol}[A]N_{ss}f_{ss} \qquad (11)$$

In eq 11, N_{ss} is the density of surface states, f_{ss} is the fraction of surface states that are filled with electrons, and k_{sol} is the electron-transfer rate constant from a surface trap to a solution acceptor. At steady state, $df_{ss}/dt = 0$, producing the following rate expression:

$$\text{rate} = k_{et}[A]n_s + k_{sol}[A]N_{ss}\left[\frac{k_{ss}n_s}{k_{ss}n_s + k_{sol}[A]}\right] \qquad (12)$$

where k_{ss} is the rate constant for transfer of an electron from the conduction band into a surface state. If an electron slowly fills a surface trap and proceeds quickly to the solution such that $k_{sol}[A] \gg k_{ss}n_s$ and k_{ss} is interpreted as a collisional event, eq 12 becomes

SCHEME 3: Two Possible Mechanisms for Interfacial Electron Transfer[a]

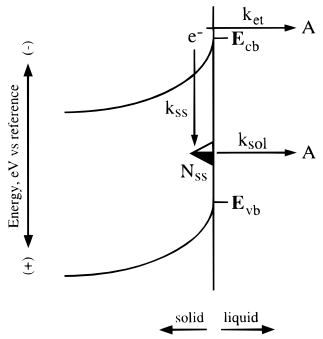

[a] The upper pathway shows the direct transfer of electrons from the conduction band edge of the semiconductor to the acceptor in solution, with the rate constant k_{et}. The lower pathway depicts the surface-state mediation of interfacial electron transfer. N_{ss} is the density of surface states, k_{ss} is the rate constant for electron capture from the conduction band into surface states, and k_{sol} is the rate constant for electon injection from the surface states into solution.

$$\text{rate} = k_{et}[A]n_s + (\sigma\upsilon)N_{ss}n_s \qquad (13)$$

where the parenthetical term is k_{ss}, σ is the cross section of a trap for charge capture, and υ is the thermal velocity of the charge carriers. The thermal velocity of electrons is well-known for n-Si to be 10^7 cm s^{-1}.[24] Equation 13 indicates that in the scenario of slow electron trapping by surface states and fast electron ejection into solution, a large N_{ss} will eliminate the dependence of J on [A]. In the converse case of fast electron trapping and a rate-determining step of electron ejection into solution such that $k_{ss}n_s \gg k_{sol}[A]$, eq 12 reduces to

$$\text{rate} = k_{et}[A]n_s + k_{sol}[A]N_{ss} \qquad (14)$$

For the rate in eq 14, a large N_{ss} will eliminate the dependence of J on n_s. Regardless of which surface-state mediation step dictates the rate, a significant density of electrical traps will at best hamper and at worst prevent steady-state measurements of k_{et}. Gerischer has suggested that redox species couple more strongly to surface states than to conduction band states, and hence, even a small N_{ss} would generally overwhelm the steady-state, electron-transfer current flow under practical experimental conditions.[16] It is thus readily possible, through improper etching, scratching of the electrode surface, use of substrates with a large density of electrical traps, or use of electrodes such as GaAs that have an inherently unstable surface termination chemistry,[51] to prepare highly defective semiconductor/liquid contacts that exhibit surface electron capture velocities that are limited only by thermionic emission of majority carriers from the bulk to the surface of the semiconductor. Obtaining direct, robust information on the rate constants of outer-sphere, interfacial charge-transfer events using steady-state $J-E$ methods requires careful control over the electrode surface condition so that the resulting surface is nearly defect-free.

In our kinetic experiments, the n-Si/CH_3OH interface displayed a negligible density of surface states. Because J varied linearly with [A], the rate given in eq 13 favors the k_{et} pathway by at least 1 order of magnitude. The condition that $N_{ss} \leq (k_{et}[A])/(10\sigma\upsilon)$ and the representative values of $k_{et} = 10^{-16}$ cm^4 s^{-1}, [A] = 10 mM = 6×10^{18} cm^{-3}, $\sigma = 10^{-15}$ cm^2, and $\upsilon = 10^7$ cm s^{-1} yield $N_{ss} \leq 6 \times 10^9$ cm^{-2}, or in other words, less than one electrical defect in every 10^5 surface atoms. In contrast, the lack of dependence of J on [A] observed for the n-WSe_2/CH_3CN interface was attributed to surface-state densities of $N_{ss} \geq 10^{12}$ cm^{-2}, and only an upper limit on the rate

constant for the direct charge-transfer pathway could be obtained from that semiconductor/liquid contact.[4]

C. Heterogeneous Charge-Transfer Rate Constants: Comparison Between Theory and Experiment. *(a) Semiclassical Approach.* The rate constant data produced a value of the maximum charge-transfer rate constant, $k_{et,max}$, of 6×10^{-17} $cm^4\ s^{-1}$. This value is consistent with expectations from a semiclassical approach to predicting such $k_{et,max}$ values.[7] An electron−ion collisional event can be described in terms of the cross section for electron capture, σ, the relative velocity of the reactants, υ, and the effective zone over which this electron transfer will take place, δ. Taking $\delta = 10$ Å, $\upsilon = 10^7$ cm s^{-1} (because the thermal velocity of electrons in the semiconductor will closely approximate the relative velocity of the reactants), and a geometric cross section for the ion that is appropriate for an off-resonance event such as electron transfer, $\sigma = 10^{-15}$ cm^2, yields $k_{et,max} = 10^{-15}$ $cm^4\ s^{-1}$. However, in the absence of solvent relaxation, the collision will be elastic and the electron will not reduce the ion. Therefore, this estimate of $k_{et,max}$, which has been described earlier,[7] should be reduced by approximately the ratio of the electronic relaxation frequency compared to the frequency factor for the solvent relaxation, i.e., by a factor of $(10^{15}\ s^{-1})/(10^{13}\ s^{-1}) = 10^2$. This yields a semiclassical estimate for $k_{et,max}$ of 10^{-17} $cm^4\ s^{-1}$, in good agreement with the experimental observations reported herein.

(b) Electronic Coupling Estimate. An alternate expression for k_{et}, adapted from a Marcus liquid−liquid relation with the donors and acceptors separated into immiscible phases,[52] is[7]

$$k_{et} = \nu_n \kappa_{el} \kappa_n \tag{15a}$$

where ν_n is the attempt frequency of the process, κ_{el} is the electronic coupling between the donor and acceptor, and κ_n is the nuclear term that contains the Franck−Condon factor for the electron-transfer event. The last two parameters are further described by

$$\kappa_{el} = \pi\left[\frac{2(r_e + r_A)}{\beta^3} + \frac{6}{\beta^4}\right] \tag{15b}$$

and

$$\kappa_n = \exp\left\{\frac{-(\lambda + \Delta G^{\circ\prime})^2}{4\lambda kT}\right\} \tag{15c}$$

where r_e is the effective radius of the delocalized donor in the semiconductor, r_A is the radius of the acceptor ion in solution, and β is the attenuation factor for the electronic overlap between the donor and acceptor in the nonadiabatic electron-transfer regime.

Since the effective Bohr radius in Si is known[28,53] and since β is roughly 1 $Å^{-1}$ for most electron-transfer systems studied to date,[20,21,54−62] use of $\nu_n = 10^{13}\ s^{-1}$, $r_e = 1 \times 10^{-7}$ cm, $r_A = 3 \times 10^{-8}$ cm, $\beta = 1 \times 10^8\ cm^{-1}$, and $\kappa_n = 1$ yields $k_{et,max} = 10^{-17}\ cm^4\ s^{-1}$. This prediction is clearly in excellent agreement with the experimental data reported herein on n-Si/CH_3OH−viologen$^{2+/+}$ contacts.

A recent paper has questioned whether the electron transfer indeed occurs nonadiabatically from a semiconductor to an acceptor in solution and has also questioned other aspects of the theory summarized above.[63] We note, however, that in fact adiabaticity has already been included in the above treatments. In the electronic coupling model, the representation of the electron as a delocalized particle having a radius greater than an atomic radius implicitly incorporates the adiabaticity of the reaction into the estimate of $k_{et,max}$.[41] Similarly, the distance of the effective reaction zone, δ, incorporates adiabaticity into the semiclassical model.[41] Addition of another separate correction to the two-sphere model, which already uses a Bohr radius to describe the electronic delocalization, seems to require careful consideration and justification.

A more refined procedure, which involves laminae instead of simple spheres and which more explicitly includes the electrons within a Bohr radius of the interface into the charge-transfer event, has been proposed recently.[64] We note, however, that any electrons that are located at distances of less than a Bohr radius from the interface will no longer experience the periodic potential of the semiconductor crystal but will instead be more localized and thus higher in energy. These localized electrons will require a more complete formulation of their effective radius, their solvation and nuclear reorganization energies, their electronic coupling parameters, etc. than is available from any theoretical description available to date. In fact, these charges more closely resemble surface states than delocalized electronic carriers in the semiconducting solid. Therefore, it is not clear that a full description of the population, kinetics, and electronic coupling parameters of this subspecies of carriers in the solid will affect significantly the order-of-magnitude estimate of $k_{et,max}$ that is produced by the two-sphere model presented above. The experimental data described above clearly are incompatible with hypotheses that $k_{et,max} > 10^{-14}$ $cm^4\ s^{-1}$ (ref 64) but are in excellent agreement with predictions that $k_{et,max} = 10^{-17}$−10^{-16} $cm^4\ s^{-1}$ according to eqs 15a−15c.

(c) Electronic Coupling Estimates of Semiconducting Electrodes Based on Coupling Values of Metal/Electrolyte Contacts. It is also possible to confirm the $k_{et,max}$ values of 10^{-17} $cm^4\ s^{-1}$ discussed above through reference to kinetic measurements at metal electrodes. An expression for the potential dependence of the charge-transfer rate at a metal electrode to a solution of randomly dissolved, outer-sphere redox acceptors may be written as[17,19,20,65]

$$\text{rate}(E) = \rho_{eff}[A]\left\{\frac{4\pi^2}{h}(4\pi kT\lambda)^{-1/2}\right\} \left\{\frac{\overline{H_{AB}^{\circ}}^2}{\beta}\right\}\int_{-\infty}^{\infty}\frac{\exp\{-(\mathbf{E} - \mathbf{E}^{\circ\prime} + \lambda)^2/(4\lambda kT)\}}{1 + \exp\{(qE + \mathbf{E}(A/A^-) - \mathbf{E})/(kT)\}}\,d\mathbf{E} \tag{16}$$

where ρ_{eff} is the effective number of states in the electrode (in units of states eV^{-1}) that participate in the charge-transfer event, h is Planck's constant, $\mathbf{E}(A/A^-)$ is the electrochemical potential for the redox couple A/A^- having a formal electrochemical potential $\mathbf{E}^{\circ\prime}(A/A^-)$, and $\overline{H_{AB}^{\circ}}^2$ is the square of the electronic coupling matrix element in a plane parallel to the solid/liquid contact, averaged over all degenerate states at each energy $\mathbf{E}$, at closest approach of the acceptor to the electrode surface.

At each distance r, the electronic coupling, $\overline{H_{AB}}^2(r)$, represents the electronic coupling matrix element averaged in a plane parallel to the solid/liquid contact over all degenerate states at energy $\mathbf{E}$. This quantity is assumed to be independent of energy over the experimental range of concern and thus can be taken out of the integral. Because the electronic coupling generally decays exponentially with β, the term $\{\overline{H_{AB}^{\circ}}^2/\beta\}$ represents the result of integrating $\overline{H_{AB}}^2(r)$ with respect to r. Similarly, the effective number of states is expected to be essentially constant over the energy range of concern, and its value also can be removed from the integral of eq 16. For the terms remaining in the integral, the numerator of the rational term describes the nuclear activation energy and the denominator describes the Fermi function occupancy of electronic states, at each energy $\mathbf{E}$.

Equation 16 also describes rigorously the theoretical expectations for interfacial charge-transfer kinetic processes at a semiconductor electrode. In this case, evaluation of the integral is somewhat different than for a metal, owing to the limited energy range over which electronic states are occupied in the conduction band of the semiconducting electrode. Evaluating this integral and extracting the rate constant $k_{et,max}$ from the resulting expression produces the following ratio of $k_{et,max}$ to $k_m(E)$:[66]

$$\frac{k_{et,max}}{k_m(E)} = D_m^{-1}\left\{\frac{\overline{H^\circ_{AB,sc}}^2}{\overline{H^\circ_{AB,m}}^2}\right\}\left\{\frac{\beta_m}{\beta_{sc}}\right\}\left\{\frac{l_{sc}}{l_m}\right\}\left\{\frac{d_m}{d_{sc}}\right\}^{2/3}\left\{\frac{\lambda_m}{\lambda_{sc}}\right\}^{1/2} I^{-1}(\lambda_m, E) \quad (17)$$

where the subscripts sc and m refer, respectively, to a semiconductor electrode and a metal electrode, and $I(\lambda_m, E)$ represents the integral in eq 16. The density of states D (in units of states cm^{-3} eV^{-1}), the effective coupling length l, and the atomic density of the electrode material d, quantify the number of states per eV that participate in the coupling event.

Assuming that the total electronic coupling to a state in the metal is similar to that of a state in the semiconductor, i.e., that $\overline{H^\circ_{AB}}^2$ is similar for a metal and for a semiconductor, and assuming that the ratios of the coupling lengths, decay lengths through the solvent, and reorganization energies in the two systems are on the order of unity, one can then estimate $k_{et,max}$ from experimental measurements of $k_m(E)$ vs E. Voltammetric data of Terrettaz et al.[23] for the reaction of freely diffusing Fe(2,2′-bipyridine)$_2$(CN)$_2^+$ on insulated Au electrodes have yielded excellent agreement with the predicted dependence of $k_m(E)$ on E (eq 16). Specifically, a value of $k_m(E) = 0.0078$ cm s^{-1} was determined at $E = -0.73$ V vs $E^{\circ\prime}(A/A^-)$, and a fit of the entire $k_m(E)$ vs E data set yielded $\lambda = 0.79$ eV for this redox couple at a Au electrode.[23] With these values for E and λ, the definite integral in eq 16 can be established numerically to be 0.195 eV for this metal/electrode interface. Extrapolation of $k_m(E)$ to zero thickness of the blocking layer can be performed using the experimentally observed exponential attenuation of the rate constant, assuming a 16-methylene-unit barrier layer and a decay constant of 1.08 per methylene unit. This yields an expected value of 2.5×10^5 cm s^{-1} for the reaction of Fe(2,2′-bipyridine)$_2$(CN)$_2^+$ at an unmodified Au electrode. Use of eq 17, with $D_m = 1.6 \times 10^{22}$ states cm^{-3} eV^{-1} for Au,[28] therefore predicts that if similar electronic coupling occurs at the metal and semiconductor surfaces, then $k_{et,max} = 9 \times 10^{-17}$ cm^4 s^{-1}. This estimate, although it involves a significant extrapolation of the experimental data from a 20 Å blocking layer thickness, provides an experimentally based, independent estimate of the $k_{et,max}$ values expected from the semiclassical and electronic coupling models discussed above. Notably, this quantum mechanically based estimate for $k_{et,max}$ is in excellent agreement with the experimental $k_{et,max}$ result obtained for the Si/liquid contacts described in this work, further validating the theory and experimental data discussed above.

D. Comparison to Other Rate Constants for Charge Transfer at Semiconductor/Liquid Interfaces. The theoretical estimates and experimental data presented in this work appear to be remarkably consistent with other kinetic data for charge-transfer processes at semiconductor/liquid junctions. For instance, scanning electrochemical microscopy techniques have been used to measure a k_{et} of 5.7×10^{-17} cm^4 s^{-1} at the p-WSe_2/H_2O−$Ru(NH_3)_6^{3+/2+}$ interface.[3] Substituting reasonable estimates of $\Delta G^{\circ\prime} = -1.09$ eV and $\lambda = 1.5$ eV[67] into eq 10 results in a $k_{et,max}$ at optimal exoergicity of 2×10^{-16} cm^4 s^{-1}. A recent study of the n-InP/CH_3OH junction estimated that $k_{et,max} = 10^{-16}$ cm^4 s^{-1} for redox couples such as dimethylferrocene$^{+/0}$ ($Me_2Fc^{+/0}$) and 1,1′-diphenyl-4,4′-bipyridinium$^{2+/+}$.[6] Differential capacitance measurements have yielded a k_{et} of 10^{-18} cm^4 s^{-1} for the p-GaAs/HCl(aq)−$Cu^{2+/+}$ interface,[5] which when corrected for the nuclear terms, also resulted in an estimate of $k_{et,max} = 10^{-16}$ cm^4 s^{-1}. It is not clear that this interface consists of an outer-sphere, nonadsorbing redox system, so the agreement in this case between theory and experiment might be fortuitous. Earlier measurements of heterogeneous electron-transfer rates at the n-ZnO/H_2O−$Fe(CN)_6^{3-/4-}$ junction yielded a k_{et} of 10^{-18} cm^4 s^{-1}.[2] This value also agrees qualitatively with theory, but like $Cu^{2+/+}$ in HCl(aq), it is not clear that $Fe(CN)_6^{3-/4-}$ is a nonadsorbing redox couple.

In several other systems, alternative pathways dominate the interfacial flux, and only upper limits on k_{et} can be established.[4,41] However, the upper bounds on k_{et} in these measurements are also consistent with a $k_{et,max}$ of 10^{-16} cm^4 s^{-1}. For example, an upper limit on k_{et} of 2×10^{-17} cm^4 s^{-1} has been established for the n-WSe_2/CH_3CN−$Me_2Fc^{+/0}$ interface through use of differential capacitance methods.[4] Assuming that $\Delta G^{\circ\prime} = -0.65$ eV and that $\lambda = 1$ eV, eq 10 yields $k_{et,max} < 7 \times 10^{-17}$ cm^4 s^{-1}. Additionally, upper bounds on k_{et} of 10^{-14}, 10^{-15}, and 10^{-20} cm^4 s^{-1} have been observed at n-GaAs/CH_3-CN−ferrocene$^{+/0}$, n-Si/CH_3OH−$Me_2Fc^{+/0}$, and oxidized n-InP/HCl(aq)−$Fe(CN)_6^{3-/4-}$ junctions, respectively.[41] A $k_{et,max}$ of 10^{-12} cm^4 s^{-1} has been reported from an analysis of p-InP/H_2O−$Fe(CN)_6^{3-/4-}$contacts,[68] and this observation was used to suggest that the theory discussed above needed major revision or correction. However, this InP rate constant has now been assigned to experimental artifacts, including corrosion of the electrode, a passivation process related to light intensity, a time dependence of the electrode decay dynamics, etc., and the rate constant measurement has been withdrawn.[69] Similarly, recent work has shown that a measurement of $k_{et} = 10^{-12}$ cm^4 s^{-1} for a p-GaAs/CH_3CN interface[70] also suffers from the experimental artifacts of adsorption, electrode passivation, etc. that prohibit the use of this system to test reliably the predictions of a theory developed to describe electron-transfer events with nonadsorbing, outer-sphere redox species.[71] Thus, it appears that to date there are no published reports, to our knowledge, of robust rate constant values for semiconductor/liquid contacts using nonadsorbing, randomly distributed, outer-sphere redox couples that contradict the theoretical estimates of $k_{et,max}$ described above.

E. Free-Energy Dependence of the Electron-Transfer Rate Constants at n-Si/CH_3OH−Viologen$^{2+/+}$ Contacts. The n-Si/CH_3OH−viologen$^{2+/+}$ contact is, to our knowledge, the first interface that has allowed a systematic study of the free-energy dependence of charge transfer from a semiconductor to a homologous series of nonadsorbing, outer-sphere redox couples. The k_{et} vs $\Delta G^{\circ\prime}$ data fit satisfactorily to a Marcus-type expression and yielded a reorganization energy of 0.7 eV with a $k_{et,max}$ of 6×10^{-17} cm^4 s^{-1}. Other fits to the data were less satisfactory because a higher $k_{et,max}$ (10^{-12} cm^4 s^{-1} or even 10^{-14} cm^4 s^{-1}) implied an unreasonably large value of λ.

Additional information on the free-energy dependence of k_{et} can be obtained by including an upper limit on k_{et} that has been established for a system with an even larger interfacial charge-transfer driving force, the n-Si/CH_3OH−$Me_2Fc^{+/0}$ contact. In this system, minority-carrier injection dominates majority-carrier transfer,[14] so only an upper limit on k_{et} can be established.[41] This upper limit on k_{et} is, however, 4×10^{-16} cm^4 s^{-1}, and the driving force of this process is 1.03−1.01 eV, as determined by C^{-2}−E plots[41] and transconductance measurements.[72] Placing this data point onto an expanded graph, Figure 9, clearly

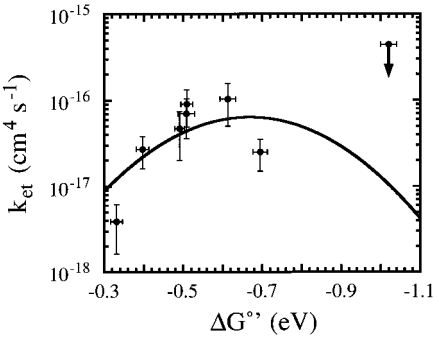

Figure 9. Experimental results of k_{et} for the n-Si/CH_3OH−bipyridinium$^{2+/+}$ systems in conjunction with the upper limit on k_{et} for the n-Si/CH_3OH−dimethylferrocene$^{+/0}$ interface (indicated by the arrow). The driving force for the k_{et} upper limit data was derived from the average barrier height for this system measured using C^{-2}−E (ϕ_b = 1.03 V[41]) and transconductance (ϕ_b = 1.01 V[72]) techniques.

constrains even further the maximum value of k_{et} for the n-Si/CH_3OH system at optimal exoergicity for an outer-sphere redox reagent.

For the n-Si/CH_3OH−viologen$^{2+/+}$ contacts, the λ of 0.7 eV from the parabolic fit to the data of Figure 8a is somewhat larger than the solution reorganization energy for the viologen redox reagents. The self-exchange rate constant, k_{se}, of the methyl viologen dication with its cation radical has been measured via electron spin resonance methods to be 2.0×10^8 M^{-1} s^{-1} in methanol.[73,74] The ionic-strength dependence of the self-exchange rate may be included to obtain a corrected rate constant, k_{corr}, using[75]

$$\ln k_{corr} = \ln k_{se} + \frac{2Z_1Z_2\alpha\sqrt{\mu}}{1 + \kappa r_r} \qquad (18)$$

where Z_1 and Z_2 are the charges on reactants 1 and 2, α is a constant with the value 1.17, μ is the ionic strength, κ equals $0.5099(\mu)^{0.5}$ Å^{-1} for CH_3OH at 25 °C, and r_r is the reactant radius, which is assumed to be identical for reactants 1 and 2. The value of λ may then be calculated from k_{corr} as follows:[76]

$$\lambda = -4kT \ln\left(\frac{k_{corr}}{Z_{bi}}\right) \qquad (19)$$

where Z_{bi} is the normal collisional vibration frequency for bimolecular reactions at room temperature. Substitution of k_{se} = 2.0×10^8 M^{-1} s^{-1}, μ = 1.0 M, and r_r = 5 Å into eq 18 and $Z_{bi} = 1 \times 10^{11}$ M^{-1} s^{-1} into eq 19 yields λ = 0.50 eV. Since most of the inner-sphere reorganization involves electrons delocalized over the bipyridine rings, it was assumed that the different functionalities did not significantly perturb this reorganization energy for the redox systems employed in this work. Moreover, the geometry of the other six compounds analogous to that of methyl viologen implies that these other compounds should have comparable outer-sphere reorganization energies. Therefore, λ for all seven compounds was estimated as ≈0.5 eV. This assumption of constant λ for the redox reagents studied in this work is implicit in the use of a single Marcus curve to compare the seven k_{et} vs $\Delta G^{\circ\prime}$ data points reported herein.

The 0.7 eV reorganization energy derived from the fit to the k_{et} vs $\Delta G^{\circ\prime}$ plot may originate from a larger reorganization energy for an acceptor in the vicinity of a semiconductor electrode than in the bulk solution, as has been postulated previously.[77,78] However, the role of both the static and high-frequency dielectric constants must be explored before this explanation can be considered rigorously.[79] In addition, the electrons in the solid may have appreciable reorganization energy due to solvation near the semiconductor/liquid interface. The results reported herein on n-Si/CH_3OH junctions cannot distinguish between these possibilities, and analogous studies on other interfaces are required to assess the generality of this observation for outer-sphere redox couples and semiconducting electrodes.

It would also be interesting to extend these kinetic measurements into the higher driving force regime in an attempt to observe the Marcus inverted region experimentally at the Si/liquid interface. Efforts to extend the 0.4 eV free energy range toward more negative $\Delta G^{\circ\prime}$ values using n-Si/CH_3OH contacts have so far been unsuccessful. Within the family of substituted bipyridinium compounds, there appears to be no reagent that has a reduction potential 0.1−0.2 V positive of the $E^{\circ\prime}$(A/A$^-$) for **VII**$^{2+/+}$ and that is also highly soluble in CH_3OH.[38] More importantly, as E(A/A$^-$) approaches the energy of the valence band edge of Si, minority-carrier processes such as bulk recombination become rate-limiting and preclude mesurement of the desired majority-carrier transfer step.[7] It is possible, however, that the use of a wider-bandgap semiconductor would eliminate this problem, and such measurements are being pursued at present in our laboratory.

V. Summary and Conclusions

In this work, n-Si/CH_3OH−viologen$^{2+/+}$ contacts displayed nearly ideal energetic and kinetic behavior and allowed experimental determination of the rate constant for charge transfer between a stable, small-bandgap semiconductor electrode and a series of homologous, one-electron, outer-sphere redox couples. Differential capacitance measurements indicated that the conduction band edge of Si was fixed, to within 40 mV, as the electrochemical potential of the solution was changed by over 400 mV, indicating a lack of Fermi level pinning for this Si/liquid system. Charge-transfer rate constants for electrons reducing bipyridinium acceptors were determined to be between 10^{-18} and 10^{-16} cm^4 s^{-1}, and the dependence of k_{et} on driving force was described satisfactorily by a Marcus-type expression with a $k_{et,max}$ of 6×10^{-17} cm^4 s^{-1} and a reorganization energy of 0.7 eV. The value for $k_{et,max}$ is in accord with theoretical predictions for charge-transfer rate constants at semiconductor/liquid contacts, and this value provides insight into the factors that control back reactions and other processes involved in charge separation at illuminated semiconductor/liquid interfaces.

Acknowledgment. We thank M. C. Lonergan for obtaining the ^{1}H NMR spectra of compounds **I**, **II**, **III**, **VI**, and **VII**. This research was supported by the National Science Foundation, Grant CHE-9634152. We also acknowledge a generous gift in support of photoelectrochemistry to Caltech from the Eastman Kodak Company.

References and Notes

(1) (a) Gerischer, H. *Z. Phys. Chem.* **1961**, *27*, 48. (b) Gerischer, H. In *Advances in Electrochemistry and Electrochemical Engineering*; Delahay, P., Ed.; Wiley-Interscience: New York, 1961; Vol. 1, pp 139−232.
(2) Morrison, S. R. *Surf. Sci.* **1969**, *15*, 363.
(3) Horrocks, B. R.; Mirkin, M. V.; Bard, A. J. *J. Phys. Chem.* **1994**, *98*, 9106.
(4) Howard, J. N.; Koval, C. A. *Anal. Chem.* **1994**, *66*, 4525.
(5) Uhlendorf, I.; Reineke-Koch, R.; Memming, R. *J. Phys. Chem.* **1996**, *100*, 4930.
(6) Pomykal, K. E.; Lewis, N. S. *J. Phys. Chem. B* **1997**, *101*, 2476.
(7) Lewis, N. S. *Annu. Rev. Phys. Chem.* **1991**, *42*, 543.
(8) Bard, A. J.; Bocarsly, A. B.; Fan, F.-R. F.; Walton, E. G.; Wrighton, M. S. *J. Am. Chem. Soc.* **1980**, *102*, 3671.
(9) Wrighton, M. S. *Acc. Chem. Res.* **1979**, *12*, 303.
(10) Bard, A. J.; Wrighton, M. S. *J. Electrochem. Soc.* **1977**, *124*, 1706.

(11) Fajardo, A. M.; Lewis, N. S. *Science* **1996**, *274*, 969.
(12) Gronet, C. M.; Lewis, N. S.; Cogan, G.; Gibbons, J. *Proc. Natl. Acad. Sci. U.S.A.* **1983**, *80*, 1152.
(13) Shreve, G. A.; Karp, C. D.; Pomykal, K. E.; Lewis, N. S. *J. Phys. Chem.* **1995**, *99*, 5575.
(14) Rosenbluth, M. L.; Lewis, N. S. *J. Am. Chem. Soc.* **1986**, *108*, 4689.
(15) Morrison, S. R. *Electrochemistry at Semiconductor and Oxidized Metal Electrodes*; Plenum: New York, 1980.
(16) Gerischer, H. *J. Phys. Chem.* **1991**, *95*, 1356.
(17) Marcus, R. A. *Annu. Rev. Phys. Chem.* **1964**, *15*, 155.
(18) Bard, A. J.; Faulkner, L. R. *Electrochemical Methods: Fundamentals and Applications*; Wiley: New York, 1980.
(19) Chidsey, C. E. D. *Science* **1991**, *251*, 919.
(20) Smalley, J. F.; Feldberg, S. W.; Chidsey, C. E. D.; Linford, M. R.; Newton, M. D.; Liu, Y. P. *J. Phys. Chem.* **1995**, *99*, 13141.
(21) Finklea, H. O.; Hanshew, D. D. *J. Am. Chem. Soc.* **1992**, *114*, 3173.
(22) Richardson, J. N.; Peck, S. R.; Curtin, L. S.; Tender, L. M.; Terrill, R. H.; Carter, M. T.; Murray, R. W.; Rowe, G. K.; Creager, S. E. *J. Phys. Chem.* **1995**, *99*, 766.
(23) Terrettaz, S.; Becka, A. M.; Traub, M. J.; Fettinger, J. C.; Miller, C. J. *J. Phys. Chem.* **1995**, *99*, 11216.
(24) Sze, S. M. *Physics of Semiconductor Devices*, 2nd ed.; Wiley: New York, 1981.
(25) Chazalviel, J.-N. *Electrochim. Acta* **1988**, *33*, 461.
(26) Fonash, S. J. *Solar Cell Device Physics*; Academic: New York, 1981.
(27) Fahrenbruch, A. L.; Bube, R. H. *Fundamentals of Solar Cells: Photovoltaic Solar Energy Conversion*; Academic: New York, 1983.
(28) Kittel, C. *Introduction to Solid State Physics*, 6th ed.; Wiley: New York, 1986.
(29) Thurber, W. R.; Mattis, R. L.; Liu, Y. M.; Filliben, J. J. *J. Electrochem. Soc.* **1980**, *127*, 1807.
(30) Sze, S. M.; Irvin, J. C. *Solid-State Electron.* **1968**, *11*, 599.
(31) *Modular Series on Solid State Devices*, 2nd ed.; Neudeck, G. W., Pierret, R., Eds.; Addison-Wesley: Reading, MA, 1989; Vol. 2.
(32) Memming, R. In *Electrochemistry II*; Steckhan, E., Ed.; Springer-Verlag: New York, 1988; Vol. 143, pp 79−112.
(33) Royea, W. J.; Krüger, O.; Lewis, N. S. *J. Electroanal. Chem.*, in press.
(34) Levich, V. G. *Acta Physicochim. URSS* **1942**, *17*, 257.
(35) Nakabayashi, S.; Itoh, K.; Fujishima, A.; Honda, K. *J. Phys. Chem.* **1983**, *87*, 5301.
(36) Lu, H.; Prieskorn, J. N.; Hupp, J. T. *J. Am. Chem. Soc.* **1993**, *115*, 4927.
(37) Atomic force microscopy of the HF-etched n-Si showed that, over an area of 500 nm × 500 nm, the surface was flat to within 1 nm. The area calculated from the three-dimensional topography of the surface was thus equal to the area determined from the two-dimensional projection to within <0.1% accuracy.
(38) Bird, C. L.; Kuhn, A. T. *Chem. Soc. Rev.* **1981**, *10*, 49.
(39) Homer, R. F.; Tomlinson, T. E. *J. Chem. Soc.* **1960**, 2498.
(40) Hünig, S.; Schenk, W. *Liebigs Ann. Chem.* **1979**, 727.
(41) Pomykal, K. E.; Fajardo, A. M.; Lewis, N. S. *J. Phys. Chem.* **1996**, *100*, 3652.
(42) Bocarsly, A. B.; Bookbinder, D. C.; Dominey, R. N.; Lewis, N. S.; Wrighton, M. S. *J. Am. Chem. Soc.* **1980**, *102*, 3683.
(43) Laser, D.; Bard, A. J. *J. Phys. Chem.* **1976**, *80*, 459.
(44) Lieber, C. M.; Gronet, C. M.; Lewis, N. S. *Nature* **1984**, *307*, 533.
(45) Tomkiewicz, M. *Electrochim. Acta* **1990**, *35*, 1631.
(46) Nagasubramanian, G.; Wheeler, B. L.; Fan, F.-R. F.; Bard, A. J. *J. Electrochem. Soc.* **1982**, *129*, 1742.
(47) Nagasubramanian, G.; Wheeler, B. L.; Bard, A. J. *J. Electrochem. Soc.* **1983**, *130*, 1680.
(48) Nagasubramanian, G.; Wheeler, B. L.; Hope, G. A.; Bard, A. J. *J. Electrochem. Soc.* **1983**, *130*, 385.
(49) Kobayashi, H.; Takeda, N.; Sugahara, H.; Tsubomura, H. *J. Phys. Chem.* **1991**, *95*, 813.
(50) Rosenwaks, Y.; Thacker, B. R.; Bertness, K.; Nozik, A. J. *J. Phys. Chem.* **1995**, *99*, 7871.
(51) Heller, A. In *Photoeffects at Semiconductor-Electrolyte Interfaces*; Nozik, A. J., Ed.; ACS Symposium Series 146; American Chemical Society: Washington, DC, 1981; pp 57−77.
(52) Marcus, R. A. *J. Phys. Chem.* **1990**, *94*, 4152.
(53) Ibach, H.; Luth, H. *Solid-State Physics*; Springer-Verlag: Berlin, 1990.
(54) Miller, J. R.; Beitz, J. V.; Huddleston, R. K. *J. Am. Chem. Soc.* **1984**, *106*, 5057.
(55) Domingue, R. P.; Fayer, M. D. *J. Chem. Phys.* **1985**, *83*, 2242.
(56) Oevering, H.; Paddon-Row: M. N.; Heppener, M.; Oliver, A. M.; Cotsaris, E.; Verhoeven, J. W.; Hush, N. S. *J. Am. Chem. Soc.* **1987**, *109*, 3258.
(57) Penfield, K. W.; Miller, J. R.; Paddon-Row, M. N.; Cotsaris, E.; Oliver, A. M.; Hush, N. S. *J. Am. Chem. Soc.* **1987**, *109*, 5061.
(58) Closs, G. L.; Miller, J. R. *Science* **1988**, *240*, 440.
(59) Elias, H.; Chou, M. H.; Winkler, J. R. *J. Am. Chem. Soc.* **1988**, *110*, 429.
(60) Isied, S. S.; Vassilian, A.; Wishart, J. F.; Creutz, C.; Schwarz, H. A.; Sutin, N. *J. Am. Chem. Soc.* **1988**, *110*, 635.
(61) Schanze, K. S.; Sauer, K. *J. Am. Chem. Soc.* **1988**, *110*, 1180.
(62) Bowler, B. E.; Raphael, A. L.; Gray, H. B. *Prog. Inorg. Chem.* **1990**, *38*, 259.
(63) Smith, B. B.; Halley, J. W.; Nozik, A. J. *Chem. Phys.* **1996**, *205*, 245.
(64) Smith, B. B.; Nozik, A. J. *Chem. Phys.* **1996**, *205*, 47.
(65) Levich, V. G. In *Advances in Electrochemistry and Electrochemical Engineering*; Delahay, P., Ed.; Wiley-Interscience: New York, 1966; Vol. 4, pp 249−371.
(66) Royea, W. J.; Fajardo, A. M.; Lewis, N. S. *J. Phys. Chem.*, in press.
(67) In these experiments, the valence band edge potential was observed to be +0.86 V vs SCE, while the formal potential of $Ru(NH_3)_6^{3+/2+}$ was −0.23 V vs SCE. The driving force for hole transfer is therefore $qE^{o\prime}(A/A^-) - \mathbf{E}_{vb} = -1.09$ eV. The self-exchange rate constant, corrected for the ionic-strength dependence, has been reported as $k_{corr} = 5 \times 10^4$ M^{-1} s^{-1} (Weaver, M. J.; Yee, E. L. *Inorg. Chem.* **1980**, *19*, 1936). Substitution of this value for k_{corr} with $Z_{bi} = 1 \times 10^{11}$ M^{-1} s^{-1} into eq 19 yields $\lambda = 1.5$ eV.
(68) Rosenwaks, Y.; Thacker, B. R.; Nozik, A. J.; Ellingson, R. J.; Burr, K. C.; Tang, C. L. *J. Phys. Chem.* **1994**, *98*, 2739.
(69) Nozik, A. J. Presented at the 211th National Meeting of the American Chemical Society, New Orleans, LA, March 1996; Paper PHYS 11.
(70) Rosenwaks, Y.; Thacker, B. R.; Ahrenkiel, R. K.; Nozik, A. J. *J. Phys. Chem.* **1992**, *96*, 10096.
(71) Bansal, A.; Tan, M. X.; Tufts, B. J.; Lewis, N. S. *J. Phys. Chem.* **1993**, *97*, 7309.
(72) Laibinis, P. E.; Stanton, C. E.; Lewis, N. S. *J. Phys. Chem.* **1994**, *98*, 8765.
(73) Dai, S. Ph.D. Thesis, University of Tennessee, Knoxville, 1990.
(74) Williams, F. Electron Spin Resonance Spectroscopic Studies of Radical Cation Reactions. Report 91015008; U.S. Department of Energy: Washington, DC, 1991.
(75) Wherland, S.; Gray, H. B. *Proc. Natl. Acad. Sci. U.S.A.* **1976**, *73*, 2950.
(76) Marcus, R. A. *J. Phys. Chem.* **1963**, *67*, 853.
(77) Smith, B. B.; Koval, C. A. *J. Electroanal. Chem.* **1990**, *277*, 43.
(78) Marcus, R. A. *J. Phys. Chem.* **1990**, *94*, 1050.
(79) Tan, M. X.; Lewis, N. S. *Inorg. Chim. Acta* **1996**, *242*, 311.